Detrital Zircon Geochronology and Provenance Analysis of Scotland Group Sediments, Barbados

Evan Sniderman

Advisor: Mark Brandon
Second Reader: David Evans

May 1, 2013

A Senior Thesis presented to the faculty of the Department of Geology and Geophysics, Yale University, in partial fulfillment of the Bachelor's Degree.

1. Abstract

Sedimentary formations in the Scotland Group, Barbados, are recognized as part of a unique exposure of a greater accretionary wedge known as the Barbados Ridge Complex, formed at the convergent boundary between the Caribbean and South American plates. The predominantly deep-sea turbidite beds are notoriously faulted and folded as a result of subduction and accretion, and age relations are only loosely constrained. However, comparison of previous fission track and $^{206}Pb/^{238}U$ ages of detrital zircons obtained from studies of sediments throughout the Caribbean indicates a prevailing regional connection to South American continental-derived sources. Specifically, ages of bedrock from the Guiana Highlands and Venezuelan Andes closely match detrital ages of sediments from the Maracaibo Basin, Trinidad, Margarita Island, and Barbados.

We present new $^{206}Pb/^{238}U$ and $^{207}Pb/^{206}Pb$ ages for detrital zircons from four sandstone samples of the Scotland Group's Walker's, Murphy's, and Mount All Members, all of Paleogene age. $^{206}Pb/^{238}U$ and $^{207}Pb/^{206}Pb$ ages were obtained from ICP-MS spot measurements. Zircons with concordant ages were combined with existing $^{206}Pb/^{238}U$ detrital zircon data from a provenance study by Xie et al. (2010) on the wider Caribbean region. Provisional conclusions on Barbadian and Caribbean sedimentary provenance are extended through a nonnegative factorization of inferred grain age distributions to mimic efficient source age distributions. Results suggest that as few as three primordial age distributions underpin the vast majority of variance in grain age distribution amongst twelve total samples. Further, these age distributions are closely associated with ages of particular South American bedrock units in the Guiana Shield, Northern Venezuelan Andes, and Cordilleran range on the present-day Colombia-Venezuela border. The best-fit combinations of source material describing grain provenance help to explain sequential formation of the Barbados Ridge accretionary wedge and provide evidence of diverse depositional histories and possible sedimentary reworking between Walker's and Mount All beds.

2. Introduction

Barbados represents the highest point of an underwater accretionary sediment pile that stretches from the Puerto Rico Trench to the islands of Trinidad and Tobago (Westbrook, 1982). The island lies near an active convergent boundary, and as the South American plate subducts beneath the Caribbean plate, sedimentary material is scraped off the South American plate and assimilated into the wedge. This material slowly accretes beneath and uplifts the island. The Scotland Group, named for its prominent exposure in the Scotland District in northeast Barbados, contains predominantly thick beds of coarse sandstone and clay that derive from this accretionary process and uplift (Harrison and Jukes-Browne, 1890). Though Pleistocene corals cover the majority of the island, the Scotland Group beds are particularly well exposed due to their over 300-meter elevation as well as associated subaerial erosion (Senn, 1940).

Sedimentary beds in the Scotland Group are infamously faulted and contain complicated folds. Their age relations are at present loosely constrained to Paleogene age. The overall stratigraphic sequence of the island has been divided into five formations according to lithology, structure, and paleontology, and consist of the Scotland formation, Joe's River formation, Oceanic formation, Bissex Hill marl, and overlying Pleistocene coral rock (Senn, 1940). The nature of proposed sedimentary accumulation in an accretionary wedge setting, however, complicates bed relations, and would suggest thrust fault-bounded packets of material exhibiting younger age characteristics lying stratigraphically below older packets (Speed and Larue, 1982). Indeed, interpretations of seismic reflection profiles measured across the Barbados Ridge at several locations indicate the existence of such thrust stacks along the entire length of the ridge, which thus disturb original superposition of strata (Chase and Bunce, 1969). The coincidence of incoherent seismic reflectors below stratified sediment piles, inferred low-density of the wedge from gravity modeling, and absence of high-frequency magnetic anomalies additionally confirms that the wedge comprises deformed sedimentary material (Torrini, 1989). Furthermore, the age of evolution of the Barbados Ridge Complex proves difficult to deduce because of the numerous factors that determine the stages of the ridge's development. Namely, the rate of subduction, thickness of accreted sediment, extent of compaction and dewatering of previously accreted sediment, and lithology all influence the characteristic growth of the wedge over time (Westbrook, 1982). For these reasons, Speed and Larue (1982) have speculated that the Oceanic and Scotland Groups may even record synchronous periods of deposition, or that the Scotland District embodies a series of depositionally unrelated, fault-bounded packages. Widespread faults, regional folds, and similar lithology throughout the Scotland District obstruct common relative dating techniques even amongst beds lying entirely within the Scotland Group.

Deformation of beds is believed to have begun in the late Paleogene with lateral, northwest-southeast trending compression of the wedge continuing into the Pliocene epoch or even the present-day (Westbrook, 1982; Torrini, 1989; Speed and Larue, 1982). This observation relies principally on paleontological evidence, as allochthonous faunal groups present in outcropping Scotland Group beds suggest Eocene and younger ages (Caudri, 1972; Senn, 1940). In particular, examination of Foraminifera prevalent in the Scotland Group provides a constraint on age and depositional environment. Fossilized Foraminifera include genera such as *Discocyclina* and *Nummulites* that correlate with other abyssal assemblages extant in the Middle Eocene (Caudri, 1972). Trechmann (1925) also states that Scotland Group fauna "[have] much affinity with the Claiborne facies of Alabama, the Eocene of Nigeria found at Ameki, and the Lutetian and probably more to the Bartonian of Europe." The presence of these marine fauna, repeated storm-event sedimentary sequences, and poor sorting of coarse sands imply submarine fan or other marine sedimentation (Pudsey and Reading, 1982).

Even so, a poorly preserved fossil record within the Scotland Group combined with uncertain relationships between beds prohibits definitively distinguishing relative ages or depositional environments. For example, Saunders et al. (1984) note sections within the same Scotland District formation that share similar ages inferred from Foraminifera assemblages, yet which indicate possibly different prevailing paleoenvironmental conditions. If correct, their observation would suggest deposition of beds in different parts of the same basin or even in separate, smaller basins (Saunders et al., 1984). De Cizancourt (1948) additionally remarks that beds in the Upper Scotland

Formation containing the *Nummulites* genus possess characteristics indicating reworking of sediment. First, De Cizancourt (1948) notes that the fossils frequently demonstrate that they were exposed to erosion, indicating the possibility of transport after fossilization. Moreover, instances of the same fossil occur throughout the Scotland Formation, and no horizon is uniquely characterized (De Cizancourt, 1948). Rather than assign "an abnormally long vertical range to them," as Caudri (1972) describes, their ubiquity in Scotland Group beds may be more easily explained through sediment reworking. Though offering crude age and paleoenvironmental constraints, paleontological evidence falls short of precisely defining bed associations.

For these reasons, absolute rather than relative dating of sediment sources from a variety of Scotland Group beds may offer more conclusive inferences about bed relations and depositional history within the Scotland District. Sedimentary beds possessing mineral grains with comparable or disparate provenance ages may suggest correspondingly related or diverse transport histories. To this end, radiometric dating of zircon crystals can constrain the age of earliest deposition of multiple grains. Zircons preserve fission tracks at temperatures cooler than their closure temperature of approximately 200-250º C (Tagami et al., 1996). Histograms and probability density functions of cooling age distribution in different Scotland Group members can provide a measure of similarity. A fission track analysis of eight sandstone samples from the Scotland Group produced zircon cooling ages in three distinct ranges (Baldwin et al., 1986). These groupings included cooling ages from 20-80 Ma, 200-350 Ma, and greater than 500 Ma (Fig. 1).

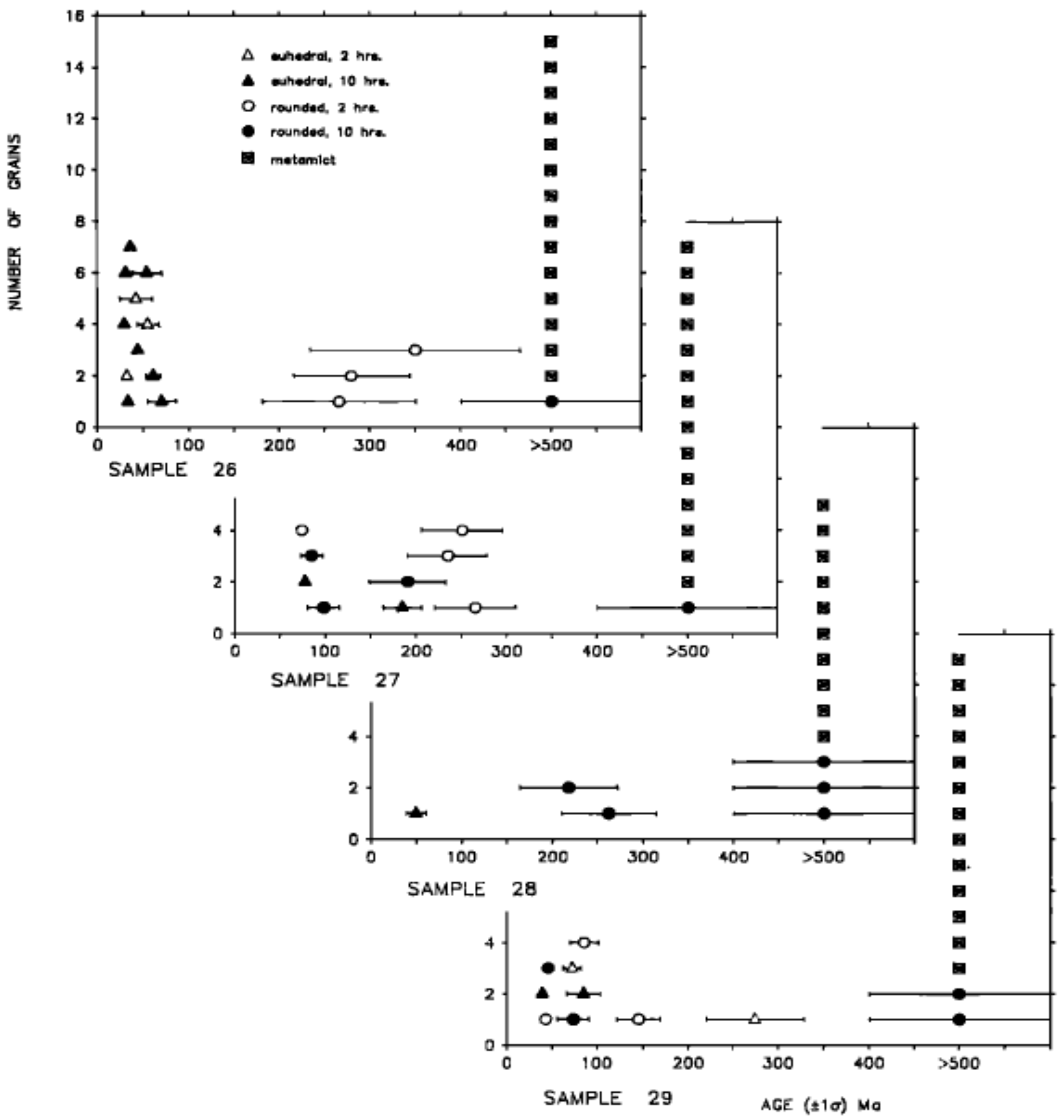

Fig. 1: Cooling ages of four zircon separates from the Scotland Group. Three groupings can be seen from 20-80 Ma, 200-350 Ma, and greater than 500 Ma in each sample (Baldwin et al., 1986).

Most grains were older than 500 Ma or were assumed to be older than 500 Ma because they contained metamict crystals. The irradiated crystals did not exhibit high enough concentrations of uranium to cause young crystals to become similarly metamict. Thus, metamictization was assumed to be a proxy for age caused by a number of decay events sufficient to destroy the crystal (Baldwin et al., 1986). Crucially, however, the study lacks more precise age data for metamict grains, so the distributions of crystals with ages greater than 500 Ma, and thus the characteristics of their provenance, remain inconclusive. Moreover, though individual sample localities are reported to include “all of Senn’s (1940) lithostratigraphic members,” no further identification or cross-referencing of provenance ages between formations is provided (Baldwin et al., 1986).

The geochemical argument advanced in Baldwin’s study places the grains’ latest cooling ages in the mid-Oligocene epoch, thereby providing an additional age constraint on Scotland Group provenance. Baldwin et al. (1986) also report, however, that under-etching of zircon crystals from one sample may have resulted in ages skewed younger than actual ages, as a fewer number of fission tracks could be counted in the crystals. Regardless of latest grain age, the three cooling age bins match closely the ages of zircon crystals from other regional highland areas, namely the Coastal Ranges in the present-day north of Venezuela, the Venezuelan Andes, and the Guiana Shield. Caribbean Highland zircons date from 20-50 Ma, Venezuelan zircons from 80-115 Ma, and Guiana Shield zircons exhibit frequent metamictization (Kohn et al., 1984a; Kohn et al., 1984b). Fission track ages present the compelling possibility that Scotland Group sediments derive from multiple areas of northern South America and that fluvial transport deposited grains in the Caribbean Sea prior to their incorporation in the accretionary wedge.

Another study by Xie et al. (2010) studies detrital zircon grains derived from the wider Caribbean region, specifically localities in Barbados, Trinidad, Margarita Island, and the Maracaibo Basin. Interpretation of zircon age distributions lends credence to the multiple source hypothesis inferred from Baldwin et al. (1986) and presents the notion that different combinations of grains derived from the same or similar source regions may be expressed in the sampled localities. The project thus extends Baldwin's (1986) study, covering a wider array of depositional locations and using $^{206}Pb/^{238}U$ and $^{207}Pb/^{206}Pb$ dates rather than fission track dates. The single sample in the study of Barbados zircon grains, BAR1, yields a median age of 1700 Ma, linking it to ages obtained from samples of the outer Guiana Shield in the Rondonian-San Ignácio and Sunsás Provinces (Tassinari and Macambira, 1999; Xie et al., 2010). Maracaibo Basin sediments fall within a wider range of younger ages, suggesting a dominant Venezuela Andes source (Fig. 2). All grains from sample BAR1 were older than 1300 Ma, falling neatly within ages obtained from other Guiana Shield samples (Xie et al., 2010). However, combining this information with dates obtained in the Baldwin et al. (1986) study suggests that the Guiana Shield was likely not the only source.

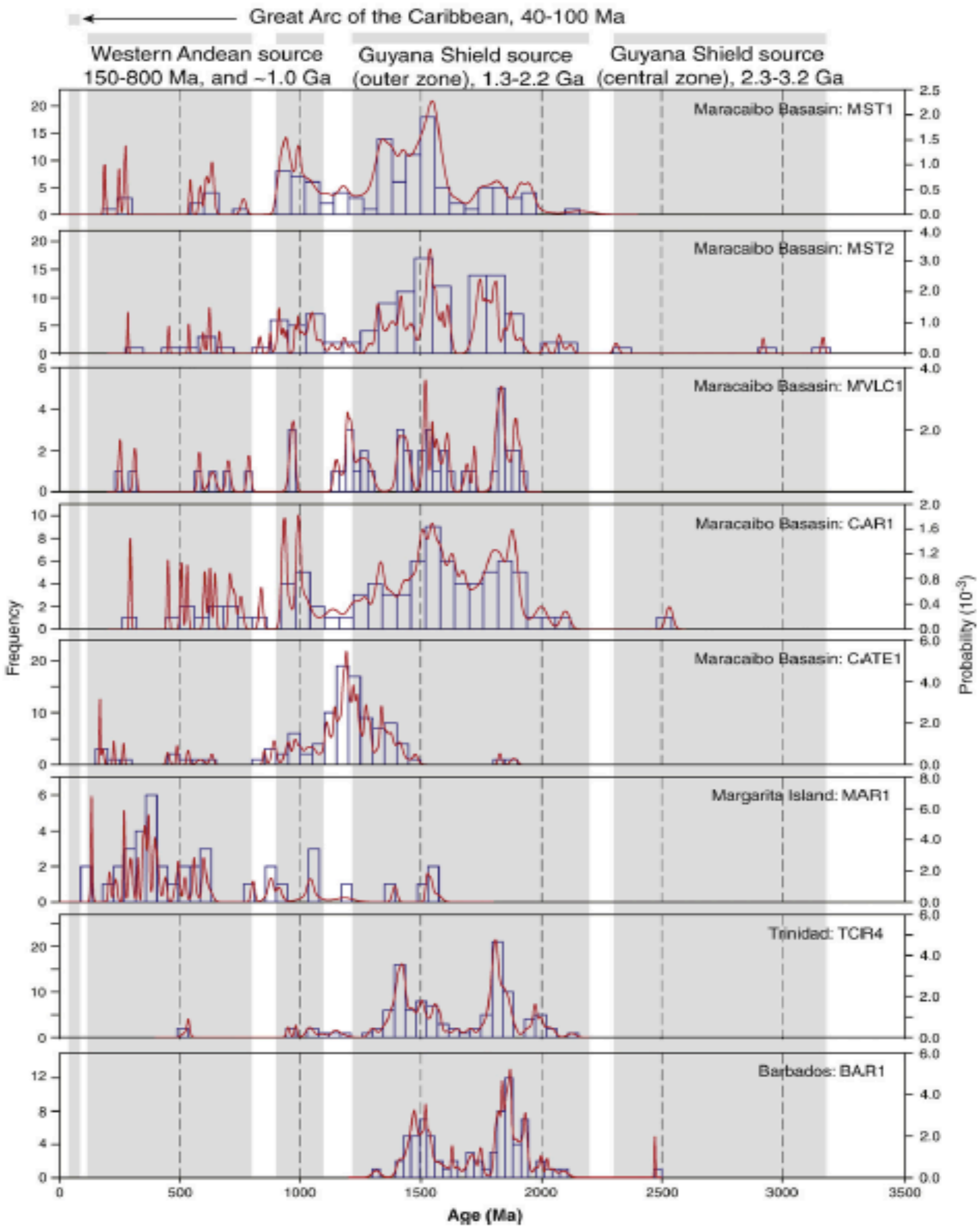

Fig. 2: Zircon grain ages from Caribbean samples (Xie et al., 2010). Authors propose Western Andean and Guiana Shield provenance.

Sample BAR1 exhibits a bimodal age distribution, which is repeated in the Trinidadian sample TCR4 and in Maracaibo Basin samples MST1, MST2, MVLC1, and

CAR1. Yet, the deficient number of Barbadian samples and the wide range of grain ages from the Maracaibo Basin preclude a correlation based simply on bimodal grain ages of the several samples. The age relations among Caribbean sediments suggest only qualitative similarities of provenance. It is worth noting that ages presented in the Baldwin et al. (1986) and Xie et al. (2010) studies are not directly comparable. As mentioned, fission track closure temperature in zircon crystals is roughly 200-250º C (Tagami et al., 1996). The lead closure temperature is comparatively higher at roughly 900º C (Cherniak and Watson, 2000). Thus, as crystals cool, the time of lead closure will predate that of fission track closure for the same grain. Grain ages reported by Xie et al. (2010), therefore, are more applicable to the current provenance study than those indicated by Baldwin et al. (1986), which undoubtedly skew the implied provenance age distribution toward younger ages. Furthermore, fission track ages are far more likely to be reset than $^{206}Pb/^{238}U$ or $^{207}Pb/^{206}Pb$ ages by sources of heat external to the system's internal crystallization and cooling process for the same reason.

Age data provided in the two studies indicate that sediments were continental-derived. Specifically, Lesser Antilles volcanic arc sediment ages scarcely coincide with those recorded in the studies. Briden et al. (1979) and Bouysse et al. (1986) confirm late Eocene ages as the oldest outer portion of the island arc (Limestone Caribbees) and 7.7 Ma and younger ages in the inner arc (Volcanic Caribbees). The vast majority of grain ages fall well outside this constraint, meaning that South American sedimentary drainage dominated Scotland Group deposition. Likely, either minimal volcanic arc-derived sediment existed at the age of deposition or trade winds blowing from consistently easterly directions disallowed deposition of arc-derived sediment in Barbados (Blume, 1974).

Paleogeographic reconstructions of Caribbean plate motion relative to the South American plate also inform provenance and age of deposition of Scotland Group sediments. For example, the Caribbean plate in the late Cretaceous and earliest Paleogene was displaced over 1000 kilometers west of its Eocene position relative to fixed South America and has moved characteristically eastward since, as depicted in

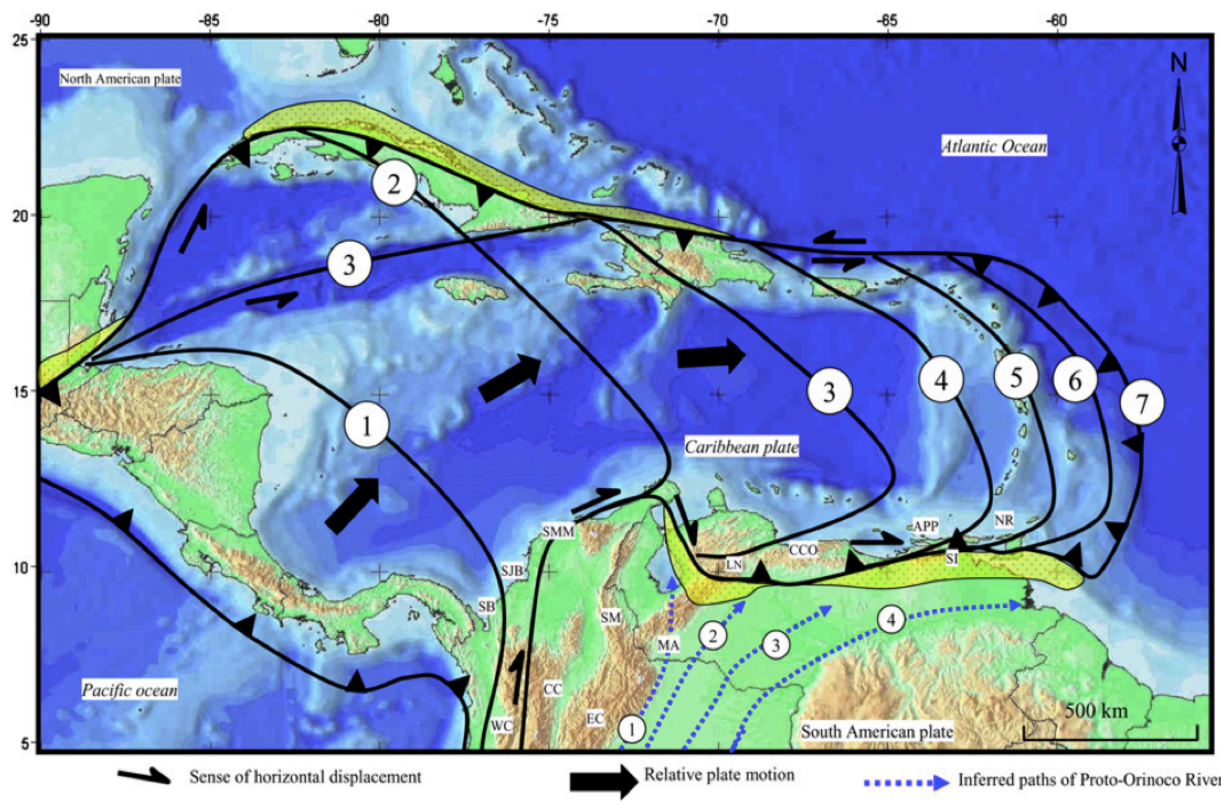

Fig. 3: Proposed paleogeographic reconstruction of Caribbean plate relative to fixed South American plate, with black lines signifying authors' interpretation of location of leading edge of Caribbean plate at sequential ages (Escalona and Mann, 2011). 1: Late Cretaceous; 2: middle Paleocene; 3: middle Eocene; 4: middle Oligocene; 5: middle Miocene; 6: Pliocene; 7: present-day.

Figure 3 (Escalona and Mann, 2011). Throughout the Cenozoic, the plate has drifted across one or more South American sedimentary drainage basins including hypothesized proto-Orinoco and proto-Maracaibo basins (Gamero, 1996). Further, according to Gamero (1996), the proto-Orinoco River may have changed course throughout the Cenozoic, having emptied into the Maracaibo Basin, the Falcon Basin, and the Eastern Venezuelan Basin. If so, sediment carried by the rerouting proto-Orinoco may have combined with sediment from several other point sources to form a line source that simultaneously deposited sediment off several locations along the northern edge of South America (Brown and Westbrook, 1987).

In any case, knowledge of the eastern extent of the Caribbean plate relative to South America throughout the Cenozoic informs relative depositional ages among beds and suggests the source areas most likely to have contributed sediment at each age. For example, the first pelagic deposits on the South American plate could have accreted to the wedge as early as Paleocene time, as the Caribbean plate is hypothesized to have traveled east relative to South America, sliding past such possible source areas as the Sinu belt, San Jacinto belt, Santa Marta massif, and the Western Cordillera (Escalona and Mann, 2011). However, the presence of such sediment in the proto-Caribbean Sea on the South American plate necessarily relies on a corresponding presence of contemporary drainage basins. A history of the Mesozoic and Cenozoic paleodrainage systems of South America constructed by Potter (1997) reveals two major events that redefined fluvial systems on the continent during these eras, namely South America's separation from Africa and Mid-Miocene Andean uplift. As the Scotland Group's depositional age is constrained to fall between these two events, as previously described, the existing paleodrainage systems after landmass breakup prove most relevant. The continental breakup caused three features that defined drainage geography: uplifts, rifting, and aulacogens (Potter, 1997). These variables shaped the principal South American watersheds and determined the relevant source areas that filled sedimentary basins in the proto-Caribbean (Fig. 4). The so-called Amazon System, Orinoco

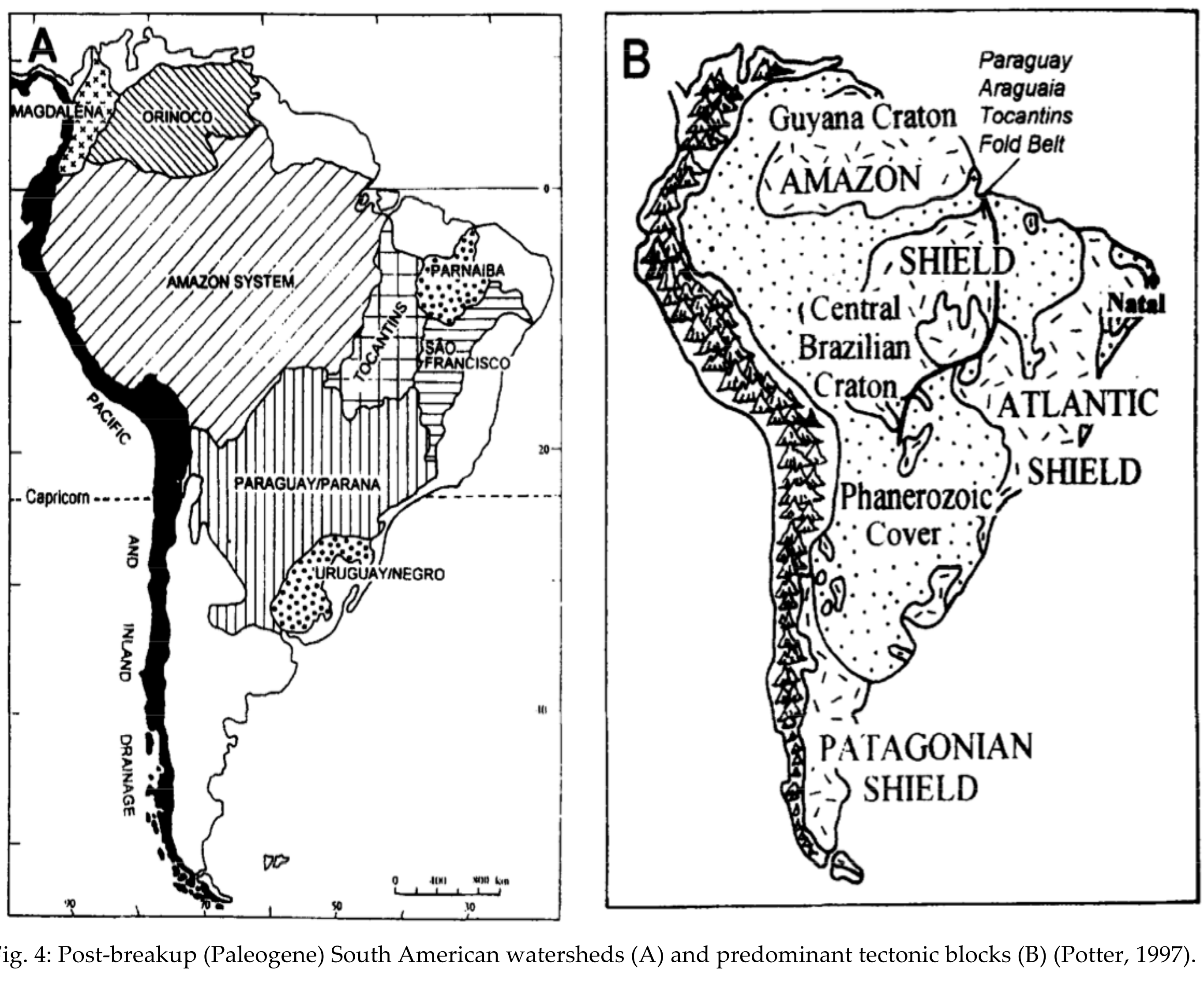

Fig. 4: Post-breakup (Paleogene) South American watersheds (A) and predominant tectonic blocks (B) (Potter, 1997).

watershed, Magdalena watershed, northern Andes, and northern coastal Maracaibo region could have provided fluvial transport of sediment from the Amazon Shield or northern Andes into the proto-Caribbean (Potter, 1997). Indeed, a large Andean geosyncline (Fig. 5b) and South American continental divide (Fig. 5a) would conceivably explain the presence of grains from these sources (Potter, 1997).

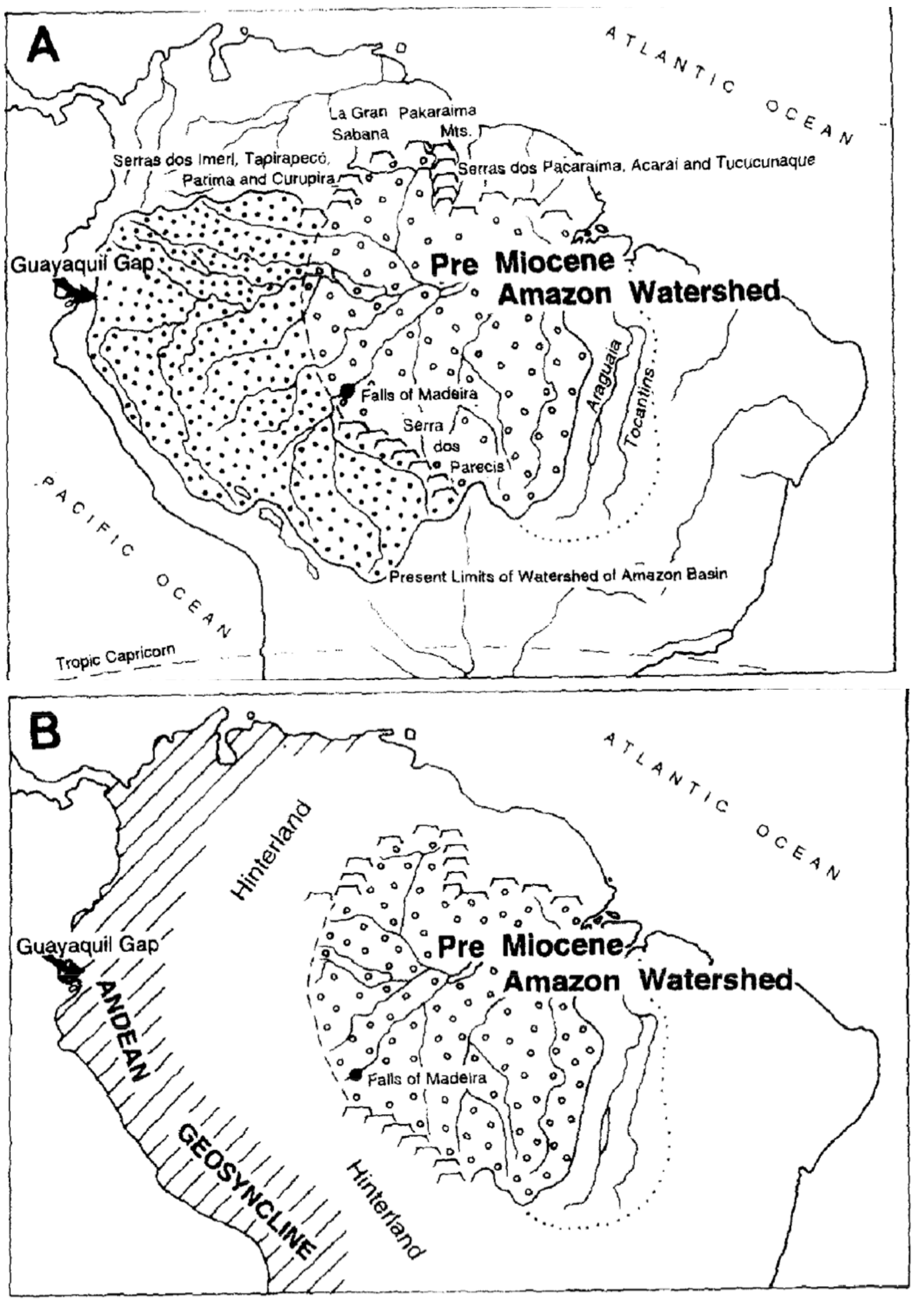

Fig. 5: Extent of Amazon watershed (A) and simplified hinterland drainage at continental divide to Andean geosyncline (B) (Potter, 1997).

In fact, Potter (1997) notes that, specifically during the interval of about 85 million years between rifting and Mid-Miocene uplift, paleodrainage into the proto-Caribbean was dominated by the northward deflection of some channels in the hinterland surrounding the Guiana Shield. Notably, north and west of the divide, channels flowed west and northwest into the Andean geosyncline (Mégard, 1987). Moreover, channels in northern South America flowed directly to the Caribbean (Nuttall, 1990; Rod, 1981). Jones (2006), citing paleontological evidence, confirms that a proto-Orinoco fluvial source likely deposited sediment into the Maracaibo Basin until the Miocene uplift. Figure 6, from

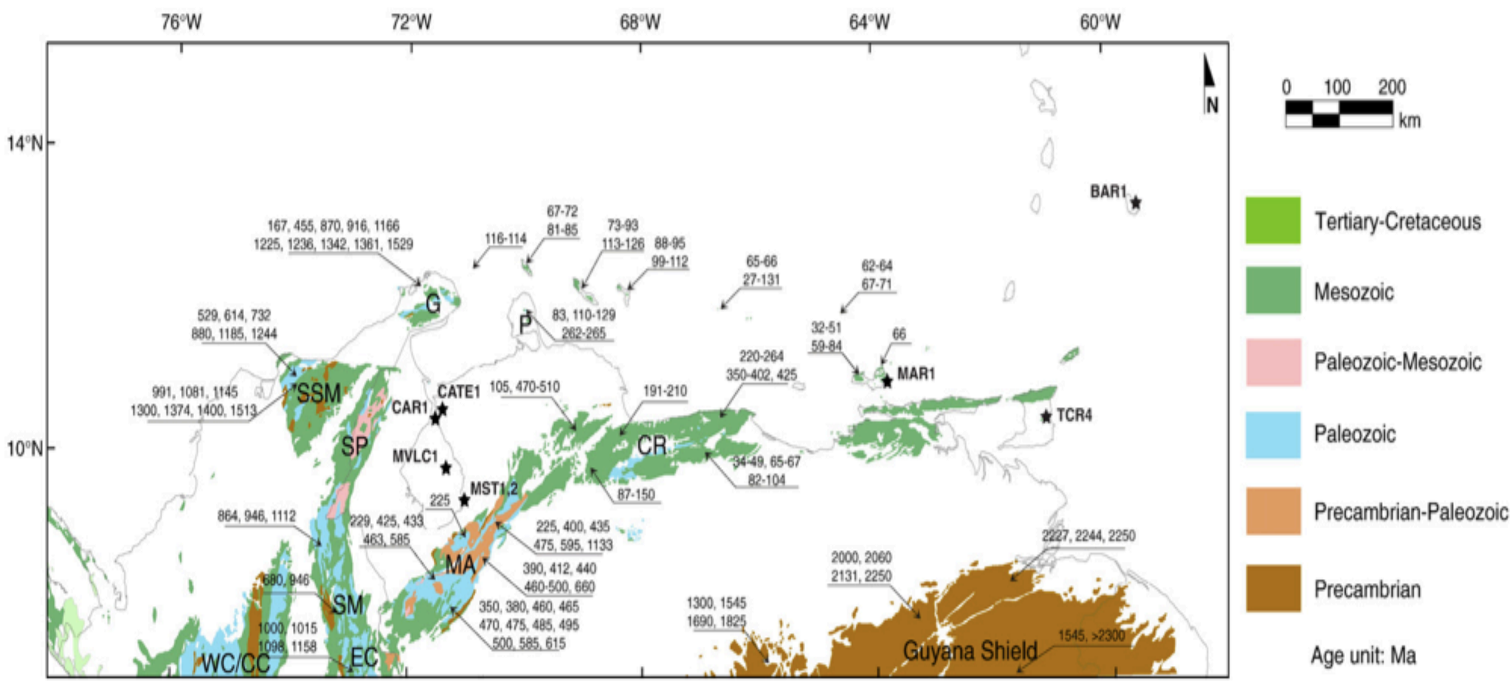

Fig. 6: Ages of basement rock units in the northern South American and Caribbean plates (Xie et al., 2010).

Xie et al. (2010), consolidates determined ages of several basement rocks from the northern South American and Caribbean plates, which likely provided source material to such channels. Sediment presumed to originate in the outer Guiana Shield has been located in the Maracaibo Basin (Xie et al., 2010). Hoorn et al. (1995) further suggest that an Amazon-Caribbean connection existed until Mid-Miocene Andean uplift, possibly providing several fluvial sources of Guiana Shield sediment to the eastern proto-Caribbean.

Combining the predominant source ages of Scotland Group beds with a comparison of relative Caribbean and South American plate motions and contemporary paleodrainage systems may offer insights into age relations among the Scotland Group formations and wider Caribbean sedimentary deposits. In the absence of specific age controls, this study uses detrital zircon geochronology of the Scotland Group's Mount All, Murphy, and Walker members to offer a characterization of depositional age relations. Further, preferred U-Pb and Pb-Pb ages are incorporated with age data from Xie et al. (2010) to augment conclusions on greater Caribbean sedimentary provenance through a factorization of grain age distributions into principal components.

3. Methods

Five detrital zircon sample localities in the Scotland District were selected to reflect a range of accepted stratigraphic positions of Scotland Group strata first characterized by Senn (1940). The highly eroded and regionally folded beds allowed location of predominantly roadside outcrops of sandstone beds from the Mount All, Murphy, and Walker Members. Geographical positioning was used to document sample coordinates, which were then checked against the 1981 United Kingdom

Fig. 7: Sample locations of ES_1, ES_3, ES_4, and ES_5 in the Scotland District, Barbados.

Directorate of Overseas Surveys geologic map of the Scotland Area to verify the members from which samples were extracted. Two samples, ES_1 and ES_2, were taken from the Mount All Member at coordinates (13.24700, -59.55229). ES_2 was excluded from further procedures to avoid mere replication of results from ES_1. The third through fifth samples, ES_3, ES_4, and ES_5, were extracted from the Mount All, Murphy, and Walker Members at coordinates (13.24291, -59.54827), (13.23312, -59.55424), and (13.25260, -59.56839), respectively (Fig. 7). All samples were taken from fine- to medium-grained sandstones.

Zircon crystals were separated from the sandstone samples using a density separation technique according to methods described by Armstrong (1986). As the samples disaggregated easily from a loose matrix, a mortar and pestle were used to grind each sample into constituent grains. The ground samples were then sieved through size 34 mesh using a Ro-Tap machine to ensure that later density-dependent separation techniques did not discriminate instead by grain size. The first step of the density separation involved running the sediment over a wet, mineral processing Wilfley table, the Angus MacKirk Orofino 12 Volt Concentrating Table, and thoroughly washing and drying the table with compressed air between runs to avoid grain contamination. This resulted in a crude density separate from which predominantly dust and quartz were removed. The denser portion containing zircon grains was selected for further separation procedures.

Two stages of heavy liquids separation followed with an intermediate magnetic separation step; lithium heteropolytungstate (LST) was used first to float primarily any remaining quartz and feldspar grains, and methylene iodide (MeI) was used second to float most other unwanted material. Prior to the first, step, however, all samples were submerged overnight in hydrogen peroxide solution to dissolve clay minerals. Samples were submerged again for over twenty-four hours in a weak acetic acid solution to dissolve carbonate material. After rinsing and drying the samples, 600 mL of a low viscosity solution of LST with density approximately 2.8 g/mL were poured into a separatory funnel. Grains were carefully added to the solution and stirred for 45 minutes, or until separation was visibly complete. The denser portion was then rinsed and dried, and floating material was discarded. After LST reclamation, all glassware was washed, and the procedure was repeated for samples ES_3, ES_4, and ES_5.

Each sample was then run through the Frantz magnetic separator to remove magnetic grains and target diamagnetic zircon crystals without inclusions. The interchangeable parts of the Frantz were removed and cleaned with rubbing alcohol before each run to prevent contamination. Forward and side tilts were adjusted to 10º, and each sample was run through the magnet at gain settings of 0.5 A, 1.0 A, 1.5 A, and 2.0 A. The magnetic portion was set aside from the remaining sample at each interval, and the final, nonmagnetic portion was run through the last heavy liquids step.

The final heavy liquids step, sinking zircon grains and other miscellaneous, dense grains in MeI, was conducted entirely under a fume hood and with neoprene gloves, lab coat, and lab apron. A test tube was filled with approximately 3 mL MeI (density 3.3 g/mL), and a constriction tube was set into the test tube. Sample was poured into the constriction tube and gently agitated to sink zircon grains. A Teflon-coated knitting needle was then used to block the constriction hole, and the constriction tube was removed and placed over a paper funnel resting atop a designated MeI wash flask. This less dense portion of the sample was rinsed into the paper funnel with acetone, an MeI solvent. The paper funnel was dried under a heat lamp, and grains were transferred to a weighing paper envelope labeled "lights." Zircon and other heavy grains at the bottom of the test tube were carefully washed with acetone into a separate paper funnel atop an MeI wash flask. The paper funnel was rinsed several times with acetone and transferred beneath the heat lamp for drying. Grains were transferred to a weighing paper envelope labeled "zircons+," indicating the presence of zircon and other dense accessory minerals. Glassware was thoroughly rinsed under the fume hood with acetone and was subsequently washed and dried. The procedure was repeated for the three remaining samples. All four zircon separates were additionally transferred to clean petri dishes to verify the presence of zircon grains beneath a microscope. Zircon crystals could be seen in abundance in all four samples. The grains were transferred back into their corresponding envelopes, sealed in Ziploc bags, and labeled according to sample number.

Analysis of detrital grains was conducted at the University of California, Santa Cruz LA-ICP-MS laboratory under the direction of Dr. Jeremy Hourigan. Zircons and the few other dense minerals that sank in MeI from the four samples were mounted in rows on double-sided sticky tape using a mask cut from the tape backing film. Several standard fragments were mounted in rows at the center of the mount. The grains were then potted up in a 1″ ring-form using Struers Epofix epoxy. Cured mounts were removed from their ring forms, and the upper meniscus was cut off with a parting tool and lathe. The mount surface was lightly polished with 1500 grit paper followed by 9 mm and then 3 mm Struers polishing compounds on a LaboPol 5 lap wheel. All mounts were washed in 1% HNO_3 and rinsed in ultrapure water prior to installation in the Helex-2 volume cell.

Blocks of four each of the primary R33 (419 Ma; Black et al., 2004) and one of the secondary Plesovice (337 Ma; Slama et al., 2008) standards were run at the beginning and end of each session. Primary standards were run after every fifth and paired with secondary ratio standards after every tenth. Blocks of two primary and secondary standards were run between samples on the same mount. This protocol provided for an n = 15 age for the secondary standard, as accuracy and precision monitored for each 100-aliquot detrital sample.

Data were reduced using the Iolite add-on for Igor Pro (Paton et al., 2010). Iolite's exponential detrending algorithm based on the down-hole fractionation of standards is more robust than linear regression, ratio-of-means, and mean-of-ratios data reduction methodologies. Specifically, unknowns that exhibit different fractionation behavior from the standards maintain a temporal trend after down-hole correction resulting in a higher standard deviation when the signal is averaged. Thus, the estimate of internal precision accounts for differences in the ablation behavior of the standards and the unknowns.

Triggered acquisition and the reproducible sample washout of the Helex-2 allowed for automatic integration based on fixed time windows without modification on roughly 90% of typical samples. Integration regions were resized if either drill-through was observed based on a rapid decrease in total beam prior to the end of lasing or spikes of ^{204}Pb were observed in the background-corrected ^{204}Pb signal. Total ^{204}Pb backgrounds (Pb + Hg) are typically about 300 CPS ± 10 CPS. Other than ^{204}Pb spikes related to inclusions or correlated with high uranium zones, average background-subtracted signals are typically less than a conservatively estimated limit of detection of 3 times the standard deviation. In these cases no ^{204}Pb correction was applied, data were exported from Igor Pro, and instead the ^{207}Pb-corrected $^{206}Pb/^{238}U$ age was used, calculated with methods provided in the Isoplot V3.0 Visual Basic add-in for Microsoft Excel (Ludwig, 2003).

Because of the imprecision of $^{207}Pb/^{206}Pb$ values at young ages, $^{206}Pb/^{238}U$ ages were preferred for ages less than 1000 Ma, and $^{207}Pb/^{206}Pb$ ages were preferred for ages greater than 1000 Ma. This follows the convention used in the Xie et al. (2010) study of detrital zircons from the Caribbean region. Discordance of grain age was calculated based on the ^{204}Pb-corrected $^{207}Pb/^{206}Pb$ and ^{207}Pb-corrected $^{206}Pb/^{238}U$ ages. Grains with ±10% discordance were not included in the final interpretation of results. All calculated ages had analytical uncertainties listed as 2σ, and concordia diagrams, which can be found in the appendix, were produced in Isoplot.

Sample age distributions were produced in MATLAB from the preferred concordant ages of the four Barbadian samples as well as the eight Caribbean samples in Xie et al. (2010). The distributions are depicted on a plot with log scale to easily depict age multiples relative to uniform probability density so that excursions can be clearly seen. The kernel size was chosen such that a ± 3σ variation relative to uniform density would plot between 0 and 2 times the uniform density. Variations in grain age distribution falling above this threshold represent a significant retreat from uniform density.

Two and three explanatory age distribution components were then computed from these twelve distributions through a nonnegative matrix factorization method (Donoho and Stodden, 2003; Pauca et al., 2005). Similar to other matrix decomposition techniques, this method calculates strictly positive, endmember age distribution factors, a positive linear combination of which closely approximates the twelve sample age distributions. The nonnegative constraint on factors was chosen to reflect the purely additive nature of provenance contribution to sedimentary deposition. These primordial distributions were plotted beneath the sample distributions for visual comparison. Additionally, F ratios were calculated for up to ten such explanatory components. The declining proportion of remaining, unexplained sample variance was graphed to qualitatively depict the marginal contribution of each additional age distribution factor. Finally, bedrock ages summarized by Xie et al. (2010) were matched to the three-component provenance model. Individual bedrock dates were scored according to the dominant component in each sample and superimposed on a geographic map of South America to reveal patterns of endmember association. Individual Barbadian sample distributions as well as nonnegative factors and their geological implications are discussed in the following sections.

4. Results

4.1 Sample ES_1

This sample was collected from the Upper Scotland Group's Mount All member, a coarse, thick-bedded, poorly sorted sandstone. It was procured from a roadside outcrop off the Ermy Bourne Highway along the Scotland District's coastline. In total, 100 detrital zircon grains were analyzed from the sample, but ultimately 48 grains were chosen for final interpretation after filtering for discordance in excess of ±10%, measurement drill-through, and spikes of ^{204}Pb in the background-corrected ^{204}Pb signal. Grain data are tabulated in the appendix. Additionally, a concordia diagram including all grain ages regardless of discordance percent is presented.

The sample yields concordant ages ranging from 66.4 ± 0.6 Ma to 2047 ± 23 Ma. The age spectrum exhibits peaks at 325, 630, and 1400 Ma. About 48% of grains fall in the range from 1200 – 1600 Ma, and 23% register ages older than 1700 Ma.

4.2 Sample ES_3

This sample was also collected from the Upper Scotland Group's Mount All member and procured from a roadside outcrop off the Ermy Bourne Highway. 100 detrital zircon grains were analyzed from the sample, and 71 grains were chosen for interpretation after filtering for discordance, measurement drill-through, and spikes of ^{204}Pb in the background-corrected ^{204}Pb signal. Individual grain data and concordia are presented in the appendix.

The sample yields concordant ages ranging from 55.3 ± 0.9 Ma to 2129 ± 18 Ma. The age spectrum exhibits a peak at 1540 Ma. Roughly 72% of grains fall in the range from 1200 – 1600 Ma, and 23% are older than 1700 Ma. No grains measure ages between 55.3 and 950 Ma.

4.3 Sample ES_4

Sample ES_4 was collected from the Lower Scotland Group's Murphy's member, a medium to fine sandstone of a consistent, red-brown color including a significant minority of silt-sized grains. 100 detrital zircon grains were analyzed from the sample, and 74 grains were selected for interpretation after filtering for discordance, measurement drill-through, and spikes of ^{204}Pb in the background-corrected ^{204}Pb signal. The data and concordia are presented in the appendix.

The sample yields concordant ages ranging from 546.8 ± 4.1 Ma to 1997 ± 14 Ma. The age spectrum exhibits peaks at 1390, 1500, and 1800 Ma. Roughly 59% of grains share dates ranging from 1200 – 1600 Ma, and 36% are older than 1700 Ma. Notably, no grains of Cenozoic age are present in the concordant data.

4.4 Sample ES_5

The final sample was collected from the lowermost Lower Scotland Group's Walker's member, a medium sandstone of tannish color, from an outcrop behind St. Andrew's Church. 100 detrital zircon grains were analyzed from the sample, and 59 grains were ultimately selected for interpretation after filtering for discordance, measurement drill-through, and spikes of ^{204}Pb in the background-corrected ^{204}Pb signal. Individual grain data are tabulated and concordia presented in the appendix.

The sample yields concordant ages ranging from 80.6 ± 1.4 Ma to 1871 ± 12 Ma. The age spectrum exhibits two peaks at 670 and 1300 Ma. Roughly 27% of grains share ages between 580 and 700 Ma, 29% of grains share dates ranging from 1200 – 1600 Ma, and 14% are older than 1700 Ma.

4.5 Aggregate Age Distributions, Component Models, and Goodness of Fit

Figures 8 and 9 depict continuous grain age probability distributions (solid blue curves), individual grain ages (red circles), inferred two- and three-factor primordial distributions (solid gray curves), and best-fit grain age distributions as combinations of nonnegative factors (dashed red curves). Samples are organized on the plots such that the four novel Barbadian samples precede those from the Xie et al. (2010) study, which are listed sequentially in increasing geographic distance west of Barbados. Additionally, three horizontal lines at the bottom of each plot correspond to 0, 1, and 2 times the uniform density of each. Sections of curves crossing 2 times uniform density represent significant departures from uniform at those ages.

As is visually noticeable, best-fit grain age distributions for the two-component model are inferior predictors of actual age distributions than for the three-component model in which linear combinations of the three components more closely match observed grain age distributions. Further, while little difference is visible between the

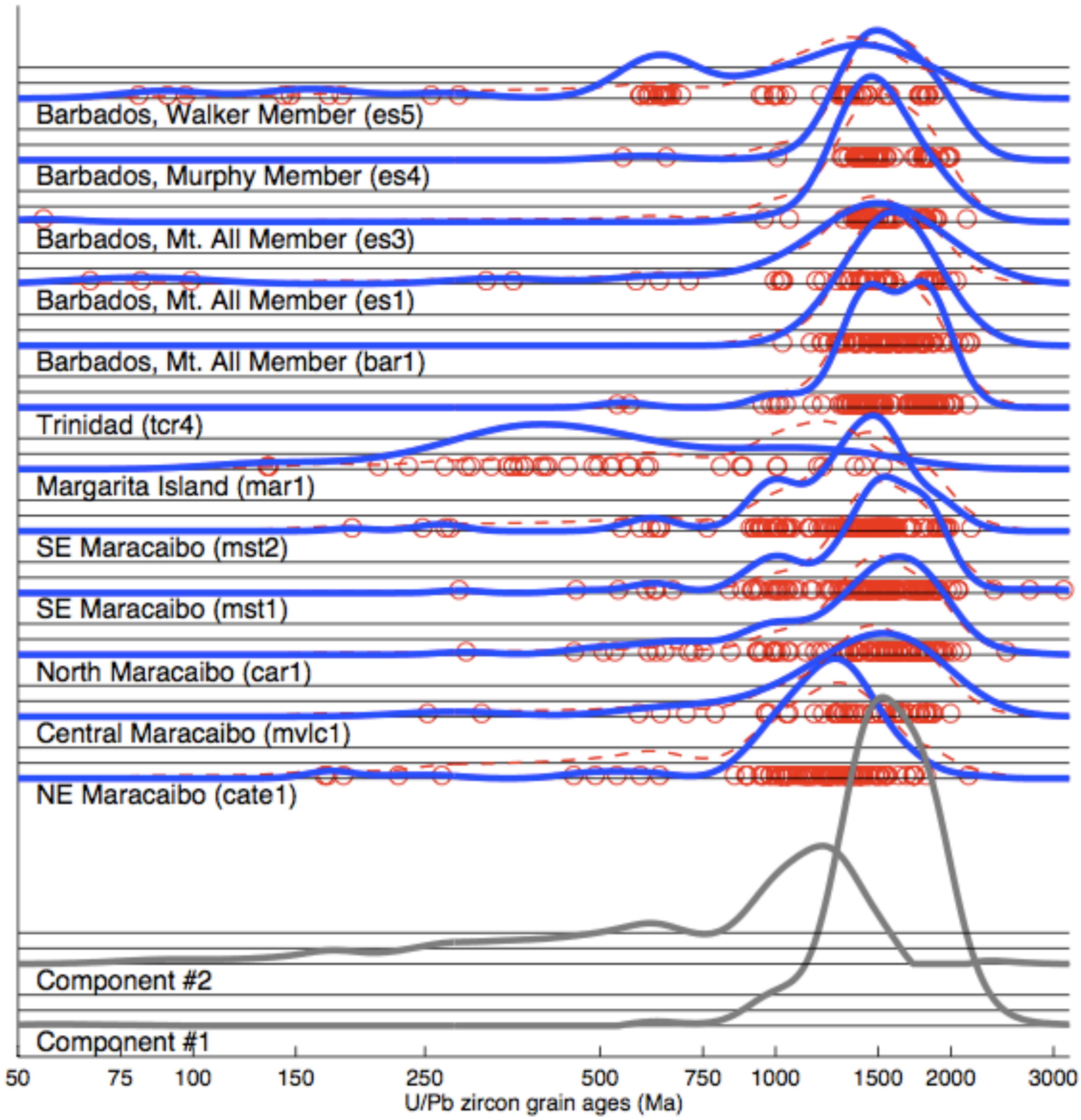

Fig. 8: Two-component factorization model of preferred zircon grain ages from Caribbean samples.

first components in either factorization, a marked discrepancy exists between the second components. In the two-component model (Fig. 8), component 2 demonstrates a steadily increasing probability distribution from 125 – 600 Ma; however, the three-component model (Fig. 9) presents a second component with minimal departures from

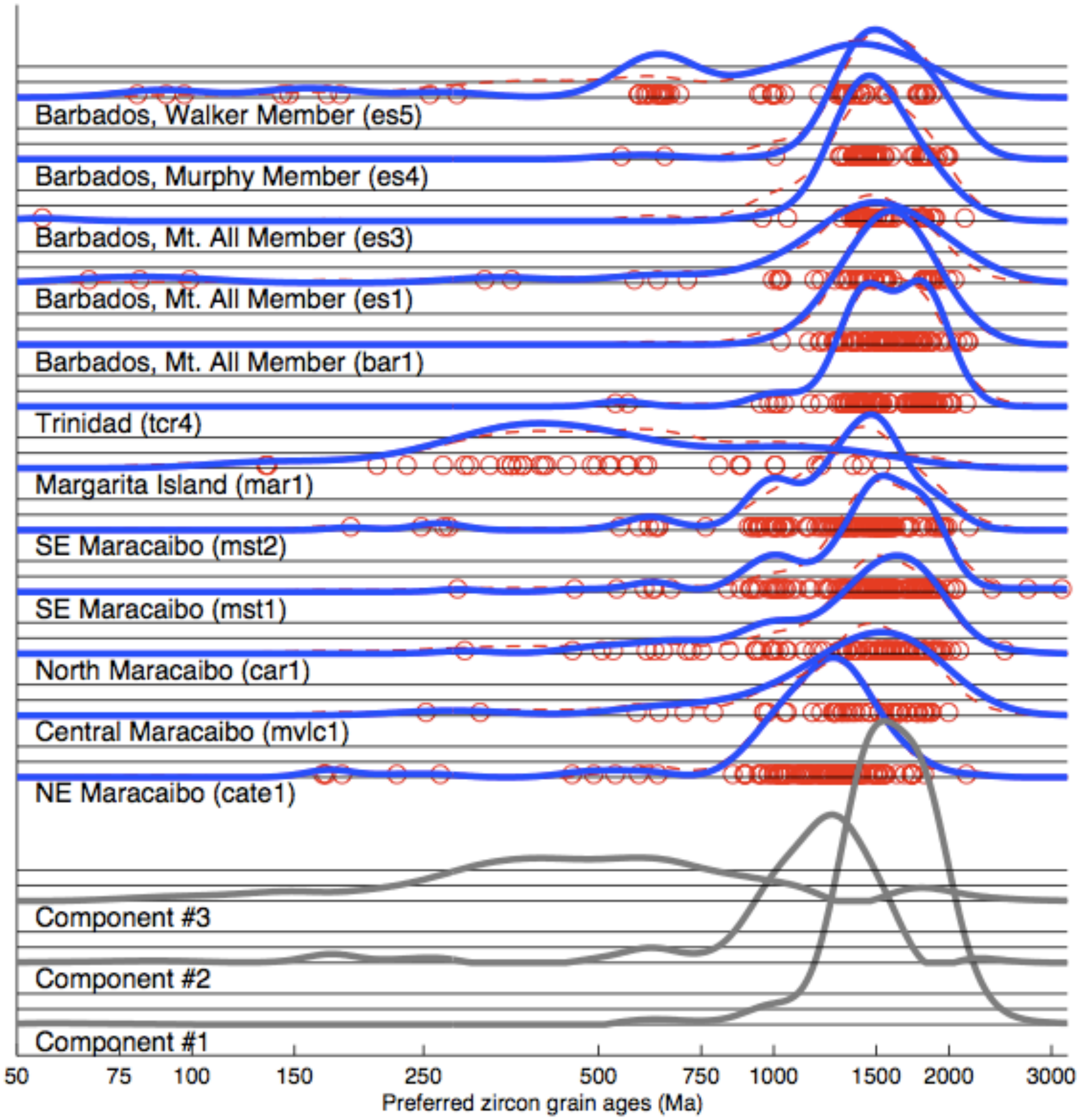

Fig. 9: Three-component factorization model of preferred grain ages.

0 times uniform density in the same age range. Rather, component 3 exhibits a broad peak centered on 500 Ma to account for distributions such as those of the Margarita Island and Barbados Walker Member samples, which possess a greater standard

deviation of grain ages younger than 600 Ma. The marginal effect of adding a third component to the predictive model may be seen in comparing the departure of component combinations from actual grain age distributions between the two figures. Samples such as ES_5, MAR1, MST2, and CATE1 are noticeably better fit with the addition of component 3. The relative weights of the three component distributions yielding the best-fit combination for each sample are expressed in Table 1.

Sample Label	Component 1 (%)	Component 2 (%)	Component 3 (%)
Barbados, Walker's Member ES_5	14	33	53
Barbados, Murphy's Member ES_4	79	21	0
Barbados, Mount All Member ES_3	60	40	0
Barbados, Mount All Member ES_1	40	39	21
Barbados, Mount All Member BAR1	86	14	0
Trinidad, TCR4	96	0	4
Margarita Island, MAR1	0	10	90
SE Maracaibo, MST2	33	60	7
SE Maracaibo, MST1	62	20	18
North Maracaibo, CAR1	48	22	30
Central Maracaibo, MVLC1	38	40	22
NE Maracaibo, CATE1	5	95	0

Table 1: Mixtures of components producing best-fit sample estimations.

A more condensed summary of the decreasing marginal model improvement due to each additional component is shown in Figure 10. An F ratio describes the reduction in unexplained variance between actual age distributions and best-fit estimations derived from linear combinations of components relative to the first nonnegative factor. The ratio is calculated as F = $\frac{RMS_i^2}{RMS_1^2}$ for the addition to the nonnegative factorization of each subsequent component i with root mean square error RMS. Each additional component after the first factor contributes less to an explanation of sample variance than the previous factor. Though the first two or three nonnegative factors contribute a significant proportion of the overall model explaining sample age variance, each factor after the third contributes a comparatively trivial amount on a marginal basis.

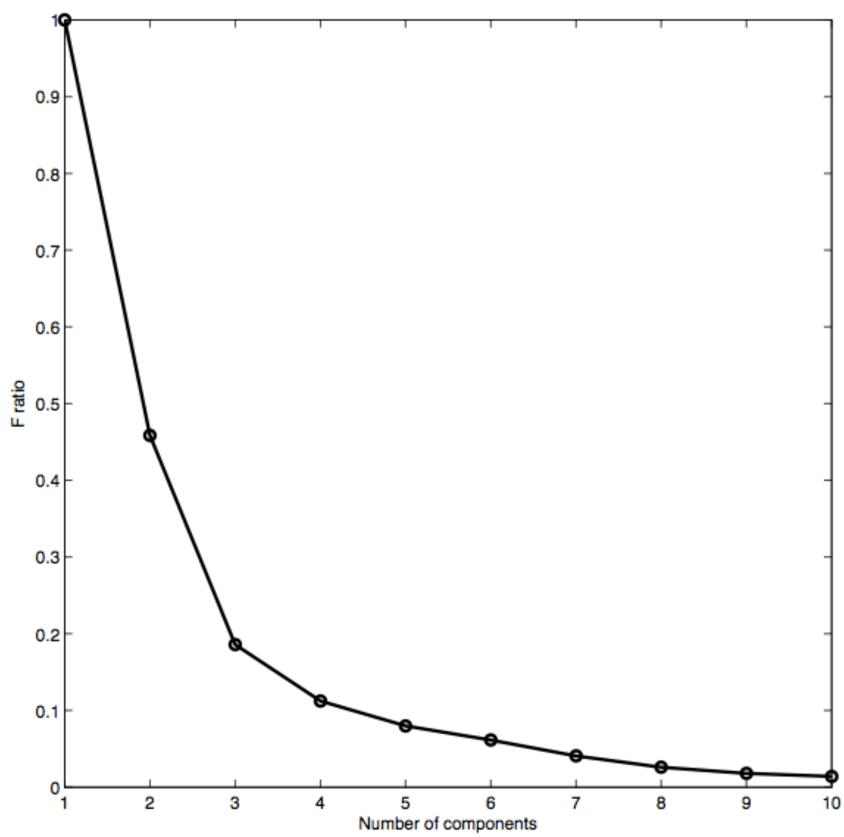

Fig. 10: Strictly declining F ratios illustrate reduction in unexplained variance associated with best-fit combinations of components.

5. Discussion

An extension of inferred nonnegative factors to the geological domain provides justification of a continental-derived three-component model of Caribbean sediment source. From the multi-component model, it is clear that no strictly positive linear combination of only one source age distribution can account for a meaningfully significant proportion of variation amongst the twelve sample age distributions. For example, ages of detrital grains from the Mount All Member sample ES_3 are strictly greater than 750 Ma, whereas a significant proportion of Margarita Island grains are younger than 750 Ma. No positive multiple of a single primordial distribution could yield both distributions. On the contrary, appealing again to Figure 10, we see that the addition of a component beyond the third contributes little additional explanatory power. Thus, two- and three-factor models appear to explain most of the variation in the twelve sample distributions.

However, close comparison of the inferred best-fit components in Figures 8 and 9 with realistic South American bedrock ages reveals the failure of the two-component model. Specifically, the second factor in the two-component model displays a nearly monotonically increasing probability density in ages 75 – 600 Ma (Fig. 8). Though such a range of bedrock ages does occur within contiguous continental sources, for example in the Guajira Peninsula and Sierra de Santa Marta in the Northern Colombian Andes (Fig. 6), no source exhibits characteristics of a smoothly increasing relative proportion of young ages in direct relation to increasing grain age (Xie et al., 2010). In other words, a distribution such as component #2 in Figure 8 holds little geological significance as a potential source age distribution. In comparison, the three-component distribution contains factors with well-defined excursions relative to uniform density that simulate ages of possible source areas (Fig. 9). The components exhibit primary peaks at 500, 1200, and 1500 Ma with differing variance and correspond to distinct, observed geological ages (Fig. 11). Though strong overlap of the three age components exists in

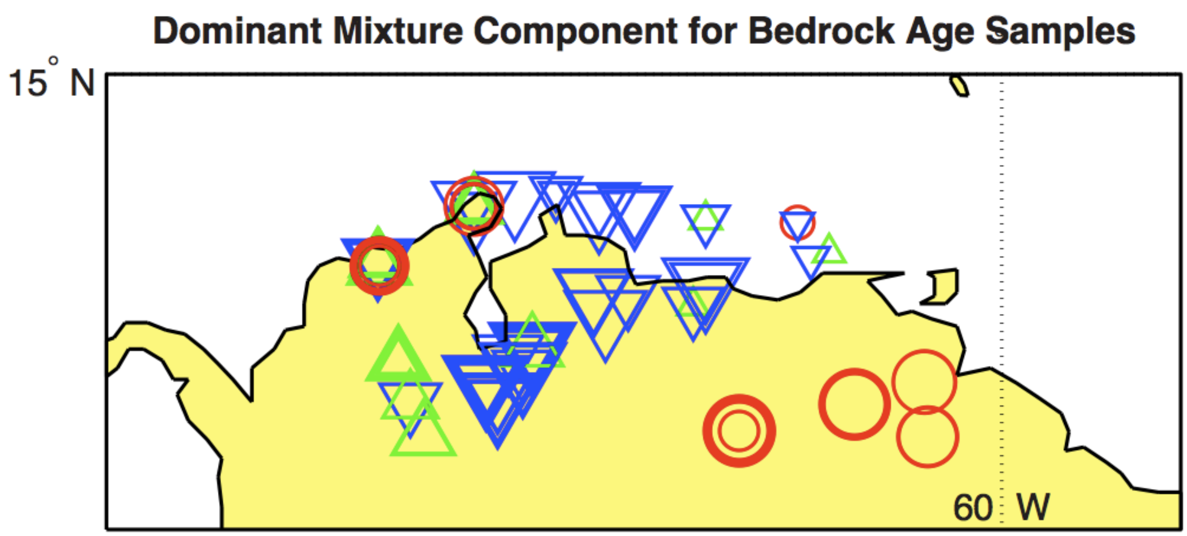

Figure 11: Filtering of South American bedrock data into three-component model according to dominant component for each age. Size of symbols scale linearly with percent of dominant component. Red circle = component #1; Green upright triangle = component #2; Blue inverted triangle = component #3.

the northern Colombian Andes, the oldest reported grain age from the northern Andean sources does not exceed 1600 Ma (Restrepo-Pace et al., 1997; Molina et al., 2006). In fact, the inner Guiana Shield is the only continental source explaining Archean material in the sampled sediments, and component #1 dominates there. Further, we find strikingly little source overlap between components 2 and 3 in the bedrock. Where overlap does exist, the percent of dominant component is still relatively low and does not suggest a source sufficiently characteristic of the inferred factor to represent the best-fit component. Rather, the Cordillera Oriental on the present-day Colombia-Venezuela border and the Northern Andean Coastal Ranges and Merida Andes in Northern Venezuela appear to independently represent components 2 and 3.

A similar reduction of detrital samples to their primary age distribution components reveals principal provenance associations (Fig. 12). While four of the five

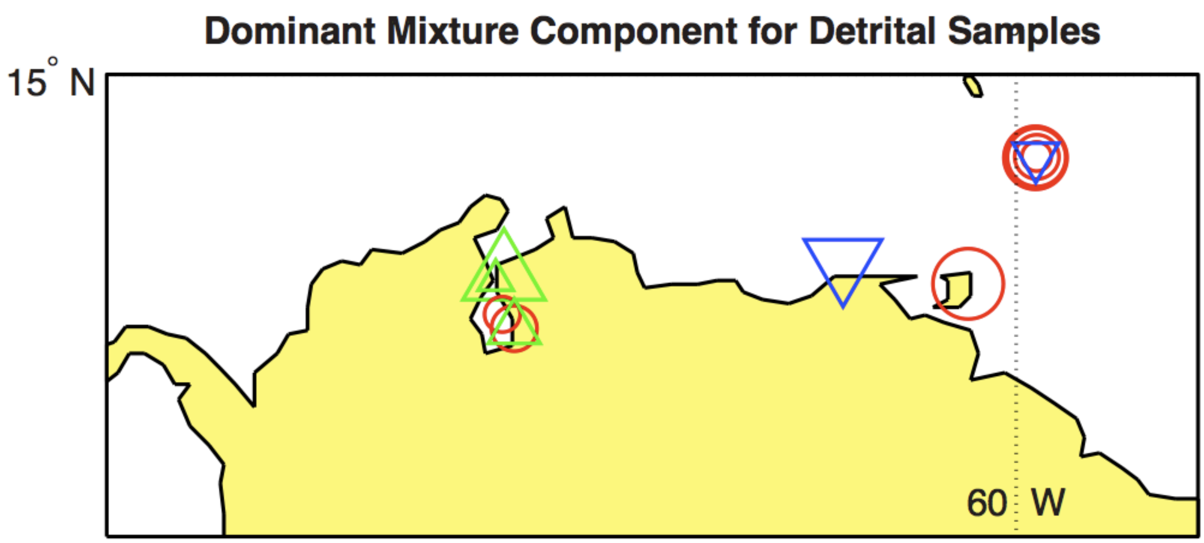

Fig. 12: Detrital samples expressed in terms of dominant component age distributions. Size of symbols scale linearly with percent of dominant component. Red circle = component #1; Green upright triangle = component #2; Blue inverted triangle = component #3.

Barbados samples exhibit a strong Guiana Shield connection, a marked departure from the single-source conclusion of Xie et al. (2010) exists in the young age affinity of the lowermost sample from the Scotland Group's Walker's Member, ES_5. In fact, strong clusters of concordant ages around 100, 200, and 600 Ma in the Walker's Member sample indicate an additional, unmistakably younger component, as Guiana Shield bedrock ages are uniformly older. Thus, the tectonic history of the island is shown to be more complex than Xie et al. (2010) indicate. The presence of old age distributions in the Maracaibo Basin potentially reaffirms westward Guiana Shield drainage indicated by Gamero (1996) and Potter (1997). The presence of intermediate ages in the Maracaibo indicates an additional Cordilleran component from northeastward flowing channels. The Trinidadian sample, obtained south of El Pilar fault, reveals a strong Guiana Shield affinity which, as the Pointe-à-Pierre sediments are also of Eocene age (James, 2005), further attests to northwest paleodrainage from the craton.

The predominance of young provenance ages on Margarita Island and in the Walker's Member constrains sedimentation scenarios. Certainly, a line source draining the Venezuelan Coastal Ranges may have deposited sediment from the younger, coastal sources (Brown and Westbrook, 1987). However, this hypothesis is rejected for the Walker's Member on the basis of paleontological evidence from Jones (2009) that suggests a Paleocene age for the member due to the presence of *Actinosiphon barbadiensis* foraminifera. Contrastingly, the line source model for Caribbean sedimentary deposition posits northward drainage into the Caribbean coinciding with the position of the Great Arc of the Caribbean during earliest Miocene time. The hypothesis is similarly rejected for Margarita Island, as plate-tectonic reconstructions show that the lower Eocene beds were located just off the Maracaibo Basin during the period of deposition (Stockhert, 1995).

Rather, the present study favors a submarine fan point source model with deep-sea sedimentary deposition similar to that described by Gamero (1996). In fact, the synthesis of disparate young and old components is supported in a seismostratigraphic study by Olmo and Castiblanco (1991), which indicates the existence of a fluvial basin extending between the Cordillera Oriental and Guiana Shield during the Eocene. Conceivably, this basin would have facilitated the transport of material from both the Coastal Ranges (component 3) as well as the Guiana Shield (component 1). Further, the basin had the proto-Orinoco, a large, low-energy river, running through its center. Olmo and Castiblanco (1991) note that this channel incorporated sediment from higher energy tributaries to both the east and west. The basin emptied into present-day Maracaibo Lake.

Results from the present study indicate a young, Coastal Range component, medium-aged Cordilleran component, and old Guiana Shield component. Very much in accord with the Olmo and Castiblanco (1991) model of Eocene paleodrainage, Cordilleran and Guiana Shield components predominate in the five Maracaibo Basin samples of Xie et al. (2010). The predominant young age component found in the Barbados Walker's Member and almost strictly older age component in Murphy's and Mount All Members may be similarly explained by proto-Orinoco transport and the existence of a connecting fluvial basin between the Guiana Shield and Cordillera Oriental. The prevalence of Coastal Range ages in the bedrock of Kasper and Larue's

(1986) and Gamero's (1996) proposed region for an Eocene distal fan could have provided sediment to the Walker's Member during the later Paleocene (Fig. 13a).

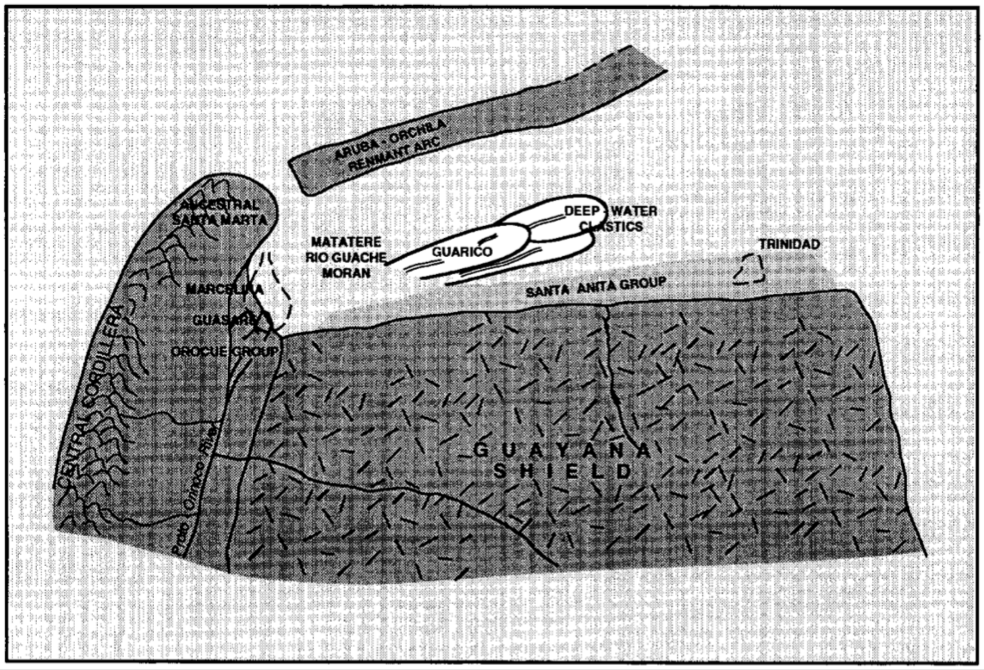

(a)

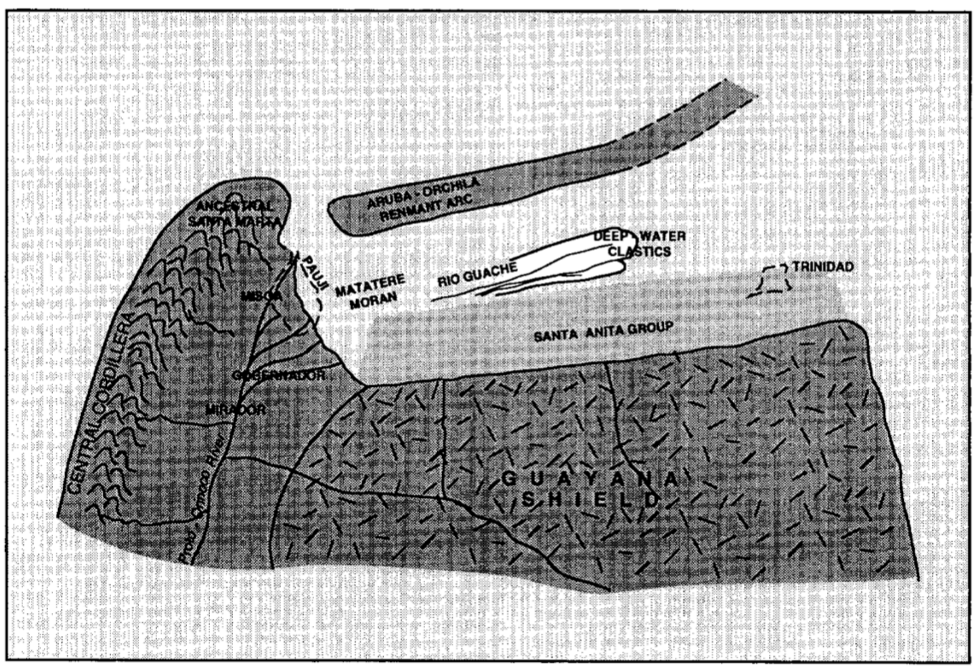

(b)

Fig. 13: Paleogeographic interpretations of Maracaibo Basin deposition from Gamero (1996). Present-day location of Trinidad and Maracaibo Lake in dashed lines. (A) Paleocene. (B) Middle Eocene.

Later assimilation of Guiana Shield sediment into the proto-Orinoco during the Eocene (Fig. 13b) would also explain the predominance of the oldest age component in the overlying Murphy's and Mount All Members. Indeed, Pudsey and Reading (1982) note several stratigraphic features attesting to the Scotland Group's belonging to the progradational fan facies. The existence of distributary channel deposits, a clear proximal and distal division of the fan, and a coarsening-upward progradational signature are present in the beds (Pudsey and Reading, 1982). ES_1, one of three total Mount All samples, expresses a minor portion of the young component in its age distribution, however. Minor sedimentary reworking within the Upper Scotland Group as corroborated by Speed and Larue (1982), De Cizancourt (1948), Caudri (1972), and Daviess (1971) may explain this minor fraction that went entirely unobserved in both the bed from which sample BAR1 was extracted and, indeed, again in a separate bed from the Mount All Member in sample ES_3. The current interpretation favors the conservation of original superpositional relationships among sequentially deposited Scotland Group members. The incorporation of a predominantly young age component from the Venezuelan Coastal Ranges is thought to have occurred first in the underlying Walker's Member, followed by the assimilation of older grains from a Guiana Shield source in the Murphy's and Mount All Members.

6. Summary

Four detrital zircon age distributions were obtained from Scotland Group sandstone samples of the Walker's, Murphy's, and Mount All Members. These distributions, when combined with eight additional age distributions of samples from the wider Caribbean region, were factored into three components that account for the majority of age variance in the twelve sample distributions. These three factors closely resemble the ages of individual bedrock units in South America, namely the Guiana Shield, Cordillera Oriental, and Coastal Ranges. Further, multiple age distribution components overlapping the same bedrock unit are generally discounted for two reasons. These units were either unable to contribute sediment to the paleodrainage basins in which samples were located or did not present a sufficiently strong characterization of the inferred factors.

A correlation of bedrock age and location with sample paleogeography and contemporary paleodrainage basins suggests that Guiana Shield, Coastal Range, and Cordilleran sediments were integrated in the Eocene epoch in the same fluvial basin fed by a proto-Orinoco source. We propose that this source fed into the Caribbean, depositing sediments from the three identified factors. The Lower Scotland Group's Walker's Member captured sediment mostly from the youngest component, whereas the Upper Scotland Group's Murphy's and Mount All Members retained sediments predominantly from the oldest component after Guiana Shield sediments were

transported to the Maracaibo Basin by the proto-Orinoco beginning in the Eocene. The small minority of young ages present in only one of four Upper Scotland Group samples is thought to represent reworking from Lower Scotland Group beds as noted by previous authors. Additional sampling from the Morgan Lewis and Chalky Mount Members of the Scotland Group is recommended to better determine trends in provenance age distribution among beds and to resolve the extent and locations of sedimentary reworking throughout the unit.

Acknowledgments

I would like to offer sincere thanks to my advisor, Mark Brandon, who was instrumental in innumerable aspects of the project, from tirelessly pursuing suitable sample localities in Barbados to advising on proper data reduction methods at Yale. Additionally, I would like to thank Keith Ma for his equally astonishingly tireless help in the separations process. Jeremy Hourigan's help in the ICP-MS laboratory at the University of California, Santa Cruz likewise could not be overstated. I would like to thank the entire Yale Department of Geology and Geophysics for the continuous guidance, fieldtrip experiences, and great times that have contributed significantly to my undergraduate experience. This thesis could not have been completed without the aforementioned help, nor would I have enjoyed so much of the process. Lastly, I would like to acknowledge the Helzer Travel Grant, which was generously provided through Silliman College, to fund costs associated with ICP-MS data collection at UC Santa Cruz.

References Cited

Armstrong, R.L., 1986. Lab Procedures for Mineral Separation at University of British Columbia.

Baldwin, S.L., Harrison, M.T., and Burke, K., 1986. Fission Track Evidence for the Source of Accreted Sandstones, Barbados. Tectonics 5.3, 457-468.

Black, L.P., Kamo, S.L., Allen, C.M., Davis, D.W., Aleinikoff, J.N., Valley, J.W., Mundil, R., Campbell, I.H., Korsch, R.J., Williams, I.S., and Foudoulis, C., 2004. Improved $^{206}Pb/^{238}U$ Microprobe Geochronology by the Monitoring of a Trace-element Related Matrix Effect; SHRIMP, ID-TIMS, ELA-ICP-MS and Oxygen Isotope Documentation for a Series of Zircon Standards. Chem. Geol. 205, 115–140.

Blume, H., 1974. The Caribbean Islands. Longman, 15-26.

Bouysse, P., Westercamp, D., and Andreieff, P., 1986. 4. The Lesser Antilles Island Arc. Proceedings of the Ocean Drilling Program: Scientific Results 110.

Briden, J.C., Rex, D.C., Faller, A.M., and Tomblin, J.F., 1979. K-Ar Geochronology and Paleomagnetism of Volcanic Rocks in the Lesser Antilles Island Arc. Philosophical Transactions of the Royal Society of London. Series A, Mathematical and Physical Sciences 291, 485-528.

Brown, K.M. and Westbrook, G.K., 1987. The Tectonic Fabric of the Barbados Ridge Accretionary Complex. Marine and Petroleum Geology 4, 71-81.

Caudri, C.M.B., 1972. The Larger Foraminifera of the Scotland District of Barbados. Eclogae Geologicae Helvetiae 65.1, 221-234.

Chase, R.L. and Bunce, E.T., 1969. Underthrusting of the Eastern Margin of the Antilles by the Floor of the Western North Atlantic Ocean, and Origin of the Barbados Ridge. Journal of Geophysical Research 74.6, 1413-1420.

Cherniak, D.J. and Watson, E.B., 2000. Pb Diffusion in Zircon. Chem. Geol. 172, 5-24.

De Cizancourt, M., 1948. Nummulites de l'Ile de la Barbade. Mém. Soc. Géol. Fr. XXVII, 57, 6-37.

Donoho, D. and Stodden, V., 2003. When Does Non-Negative Matrix Factorization Give a Correct Decomposition into Parts?

Escalona, A. and Mann, P., 2011. Tectonics, Basin Subsidence Mechanisms, and Paleogeography of the Caribbean-South American Plate Boundary Zone. Marine and Petrol. Geol. 28, 8-39.

Gamero, M.L.D., 1996. The Changing Course of the Orinoco River during the Neogene: A Review. Paleogeography, Paleoclimatology, Paleoecology 123, 385-402.

Harrison, J.B. and Jukes-Browne, A.J., 1890. The Geology of Barbados. Salisbury: Bennett Bros., Printers.

Hoorn, C., Guerrero, J., Sarmiento, G.A., and Lorente, M.A., 1995. Andean Tectonics as a Cause for Changing Drainage Patterns in Miocene Northern South America. Geology 23, 237-240.

James, K.H., 2005. A Simple Synthesis of Caribbean Geology. Caribbean Journal of Earth Science 39, 69-82.

Jones, R.W., 2006. Applied Paleontology. Cambridge University Press, Cambridge, 434.

Jones, R.W., 2009. Stratigraphy, Palaeoenvironmental Interpretation and Uplift History of Barbados Based on Foraminiferal and Other Palaeontological Evidence. Journal of Micropalaeontology 28, 37-44.

Kasper, D.C. and Larue, D.K., 1986. Paleogeographic and Tectonic Implications of Quartzose Sandstones of Barbados. Tectonics 5.6, 837-854.

Kohn, B.P., Shagam, R., Banks, P.O., and Burkley, L.A., 1984a. Mesozoic-Pleistocene Fission-Track Ages on Rocks of the Venezuelan Andes and Their Tectonic Implications. In: Bonini, W., Hargraves, R., Shagam, R. (Eds.), The Caribbean–South American Plate Boundary and Regional Tectonics. Memoir 162. Geological Society of America, 365–384.

Kohn, B.P., Shagam, R., and Subieta, T., 1984b. Results and Preliminary Implications of Sixteen Fission-Track Ages from Rocks of the Western Caribbean Mountains, Venezuela. In: Bonini, W., Hargraves, R., Shagam, R. (Eds.), The Caribbean–South American Plate Boundary and Regional Tectonics. Memoir, 162. Geological Society of America, 415-421.

Ludwig, K.R., 2003. User's Manual for Isoplot 3.00. A Geochronological Toolkit for Microsoft Excel. Berkeley Geochronology Center, Special Publication 4a, Berkeley, California.

Mégard, F., 1987. Structure and Evolution of the Peruvian Andes. The Anatomy of Mountain Ranges. Princeton University Press, Princeton, NJ.

Molina, A.C., Cordani, U.G., and MacDonald, W.D., 2006. Tectonic Correlations of Pre-Mesozoic Crust from the Northern Termination of the Colombian Andes, Caribbean Region. Journal of South American Earth Sciences 21, 337-354.

Nuttall, C.P., 1990. A Review of the Tertiary Non-Marine Faunas of the Pebasian and Other Inland Basins of Northwestern South America. Bulletin British Museum of Natural History (Geology) 45, 165-371.

Olmo, W.M.D. and Castiblanco, M., 1991. Un Modelo Paleogeográfico de la Formación Mirador (Cuenca de los Llanos, Colombia). In: 4th Simp. Boliv. Explor. Pet. Cuencas Subandinas Mem. 1.17.

Paton, C., Woodhead, J.D., Hellstrom, J.C., Hergt, J.M., Greig, A., and Maas, R., 2010. Improved Laser Ablation U-Pb Zircon Geochronology through Robust Downhole Fractionation Correction, Geochem. Geophys. Geosyst. 11.

Pauca, V.P., Piper, J., and Plemmons, R.J., 2005. Nonnegative Matrix Factorization for Spectral Data Analysis. Linear Algebra and Its Applications 416, 29-47.

Potter, P.E., 1997. The Mesozoic and Cenozoic Paleodrainage of South America: A Natural History. Journal of South American Earth Sciences 10.5-6, 331-344.

Pudsey, C.J. and Reading, H.G., 1982. Sedimentology and Structure of the Scotland Group, Barbados. Geological Society, London, Special Publications 10, 291-308.

Restrepo-Pace, P.A., Ruiz, J., Gehrels, G., and Cosca, M., 1997. Geochronology and Nd Isotopic Data of Grenville-age Rocks in the Colombian Andes: New Constraints for Late Proterozoic-Early Paleozoic Paleocontinental Reconstructions of the Americas. Earth and Planetary Science Letters 150, 427-441.

Rod, E., 1981. Notes on the Shifting Course of the Ancient Rio Orinoco from Late Cretaceous to Oligocene Time. Geos 26, 54-56.

Saunders, J.B., Bernoulli, D., Müller-Merz, E., Oberhänsli, H., Perch-Nielsen, K., Riedel, W., Sanfilippo, A., and Torrini, R. Jr., 1984. Stratigraphy of the Late Middle Eocene to Early Oligocene in the Bath Cliff Section, Barbados, West Indies. Micropaleontology 30.4, 390-425.

Senn, A., 1940. Paleogene of Barbados and its Bearing on History and Structure of Antillean-Caribbean Region. Bulletin of the American Association of Petroleum Geologists 24.9, 1548-1610.

Slama, J., Kosler, J., Condon, D.J., Crowley, J.L., Gerdes, A., Hanchar, J.M., Horstwood, M.S.A., Morris, G.A., Nasdala, L., Norberg, N., Schaltegger, U., Schoene, B., Tubrett, M.N., Whitehouse, M.J., 2008. Plesovice Zircon – A New Natural Reference Material for U-Pb and Hf Isotopic Microanalysis. Chem. Geol. 249, 1-35.

Speed, R.C. and Larue, D.K., 1982. Barbados: Architecture and Implications for Accretion. Journal of Geophysical Research 87.B5, 3633-3643.

Stöckhert, B., Maresch, W.V., Brix, M., Kaiser, C., Toetz, A., Kluge, R., and Krückhans-Lueder, G., 1995. Crustal History of Margarita Island (Venezuela) in Detail: Constraint on the Caribbean Plate-Tectonic Scenario. Geology 23.9, 787-790.

Tagami, T., Carter, A., and Hurford, A.J., 1996. Natural Long-Term Annealing of the Zircon Fission-Track System in Vienna Basin Deep Borehole Samples: Constraints upon the Partial Annealing Zone and Closure Temperature. Chem. Geol. 130, 147-157.

Tassinari, C.C.G. and Macambira, M.J.B., 1999. Geochronological Provinces of the Amazonian Craton. Episodes 22.3, 174-182.

Torrini, R. Jr., Speed, R.C., and Mattioli, G.S., 1985. Tectonic Relationships Between Forearc-Basin Strata and the Accretionary Complex at Bath, Barbados. Geological Society of America Bulletin 96, 861-874.

Trechmann, C.T., 1925. The Scotland Beds of Barbados. The Geological Magazine 62.11, 481-504.

Westbrook, G.K., 1982. The Barbados Ridge Complex: Tectonics of a Mature Forearc System. Geological Society, London, Special Publications 1982, 10, 275-290.

Xie, X., Mann, P., and Escalona, A., 2010. Regional Provenance Study of Eocene Clastic Sedimentary Rocks within the South America Caribbean Plate Boundary Zone Using Detrital Zircon Geochronology. Earth and Planetary Science Letters 291, 159-171.

Appendix

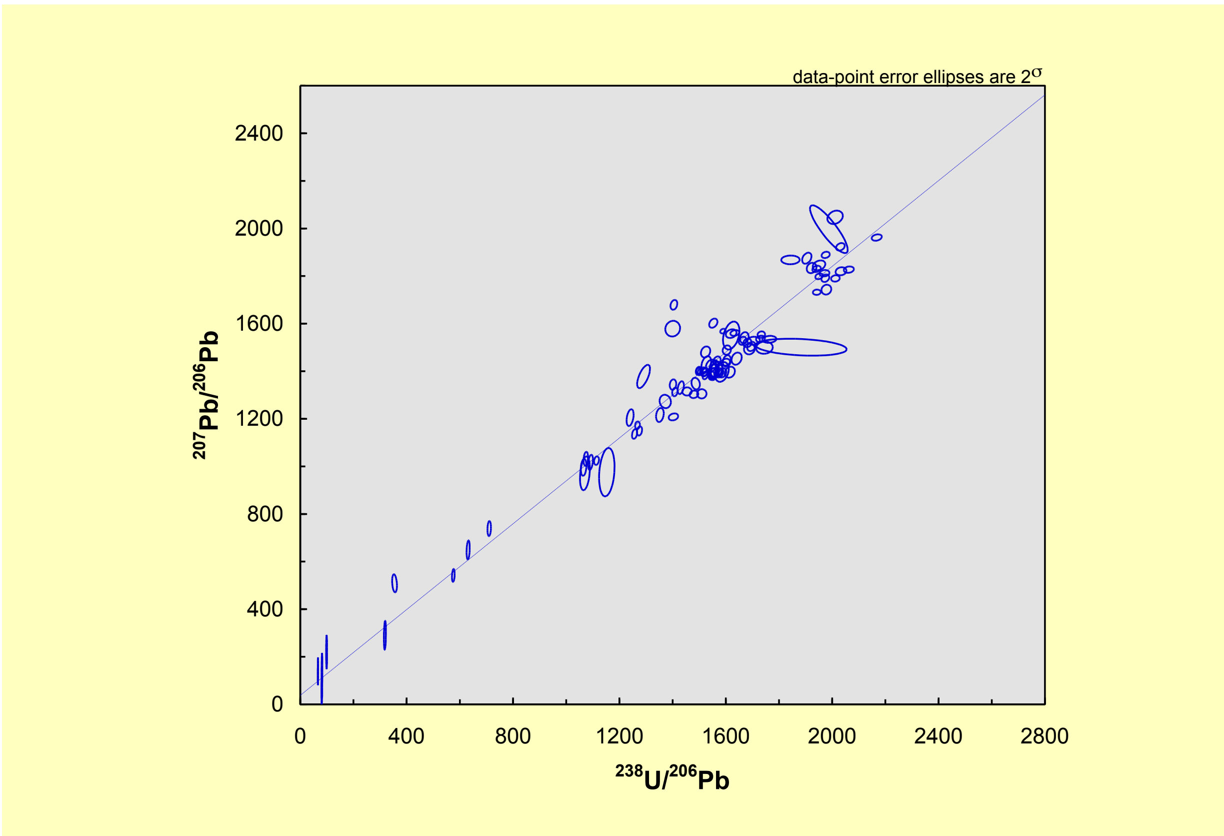

Fig. 1: Concordia plot for Mount All Member sample ES_1 data. All analyses plotted regardless of discordance, though only those within ±10% discordance are used for calculations. Age uncertainties are expressed with a 95% confidence level.

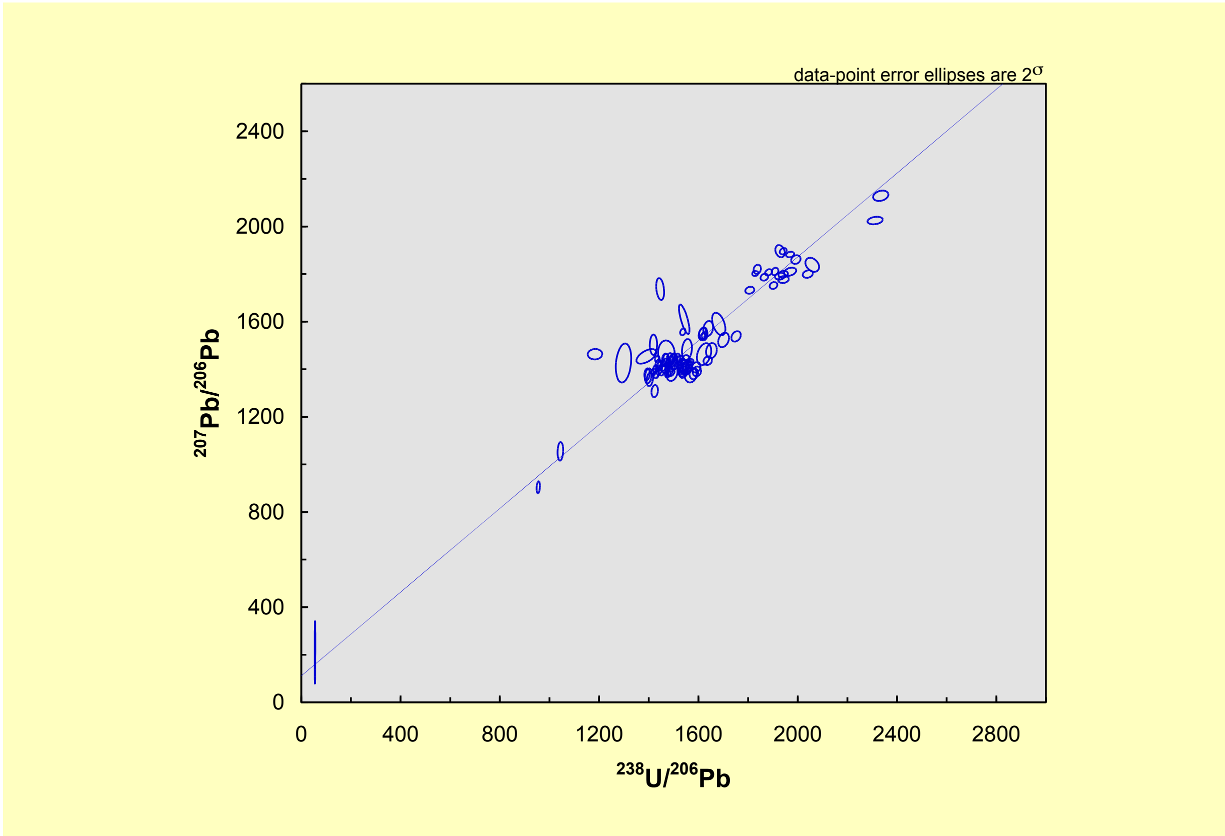

Fig. 2: Concordia plot for Mount All Member sample ES_3 data. All analyses plotted regardless of discordance, though only those within ±10% discordance are used for calculations. Age uncertainties are expressed with a 95% confidence level.

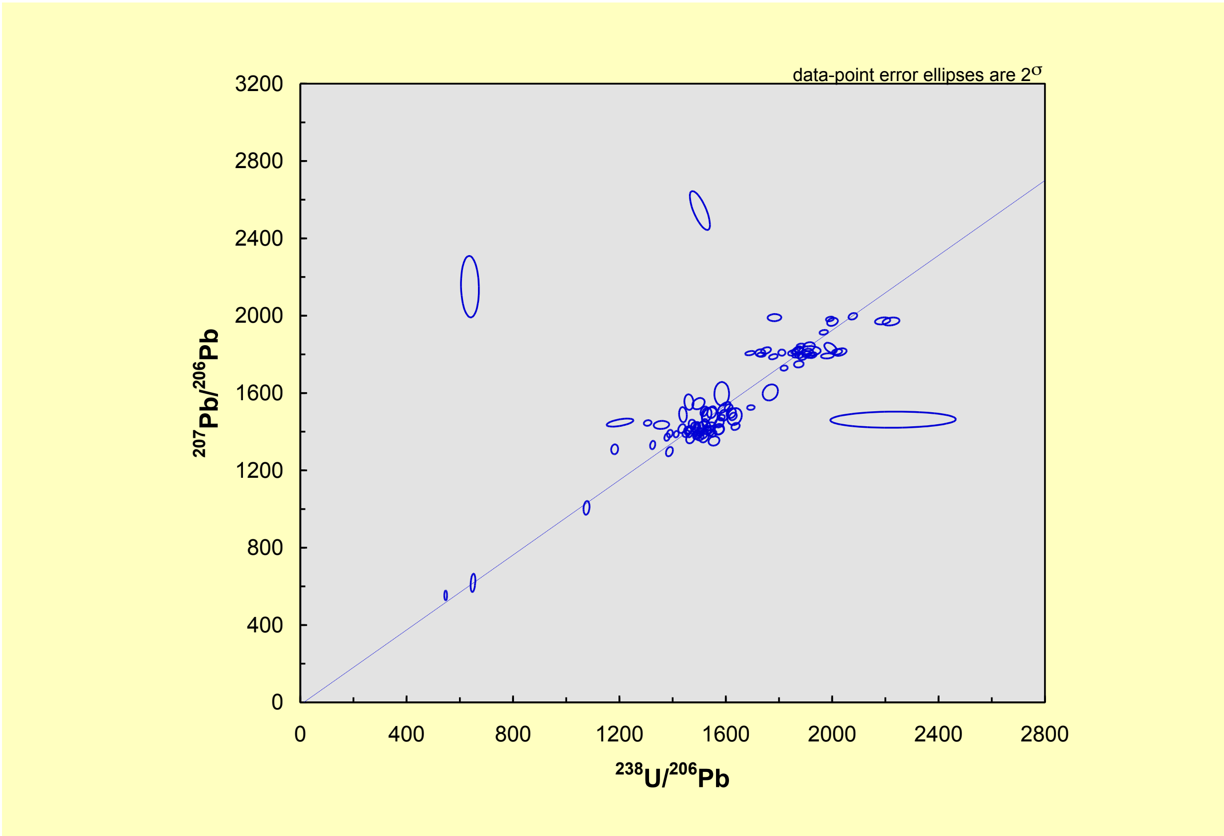

Fig. 3: Concordia plot for Murphy's Member sample ES_4 data. All analyses plotted regardless of discordance, though only those within ±10% discordance are used for calculations. Age uncertainties are expressed with a 95% confidence level.

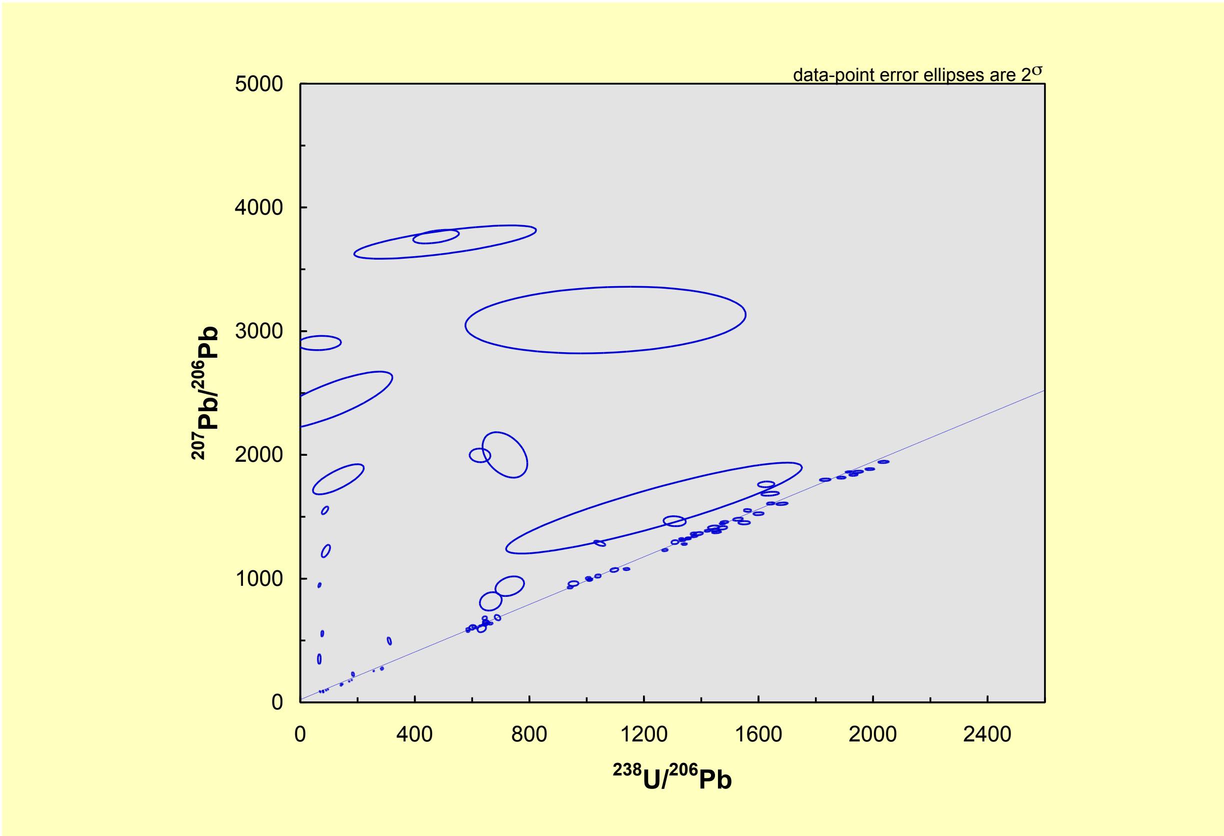

Fig. 4: Concordia plot for Walker's Member sample ES_5 data. All analyses plotted regardless of discordance, though only those within ±10% discordance are used for calculations. Age uncertainties are expressed with a 95% confidence level.

Table 1. Detrital zircon dating results for Mount All Member sample ES_1. Only grains with discordance magnitude less than 10% are used in final interpretations and probability density plots. Shaded rows indicate > 10% discordance.

Sample	$^{207}Pb/^{235}U$ ratio	2σ abs error	$^{206}Pb/^{238}U$ ratio	2σ abs error	$^{206}Pb/^{238}U$ age	2σ abs error	$^{207}Pb/^{206}Pb$ age	2σ abs error	Percent Discordant	Preferred age
ES_1_1	1.85	0.022	0.1809	0.0012	1073.7	6.9	1032	24	-4.0	1032
ES_1_2	0.875	0.014	0.10293	0.00079	631.2	4.8	649	33	0.9	631
ES_1_3	5.963	0.048	0.3673	0.0024	2030.8	13.4	1923	13	-5.6	1923
ES_1_4	3.502	0.038	0.2475	0.0019	1404.8	10.5	1679	17	16.3	1679
ES_1_5	3.216	0.028	0.264	0.0021	1519.5	11.7	1397	14	-8.8	1397
ES_1_6	2.345	0.034	0.2118	0.0019	1240.1	10.8	1205	29	-2.9	1205
ES_1_7	3.816	0.036	0.2919	0.0021	1663.0	11.7	1528	14	-8.8	1528
ES_1_8	2.923	0.031	0.2472	0.0017	1430.8	9.6	1331	22	-7.5	1331
ES_1_9	3.181	0.023	0.2612	0.0014	1503.7	7.9	1398	12	-7.6	1398
ES_1_10	2.86	0.031	0.2421	0.0018	1401.5	10.1	1344	18	-4.3	1344
ES_1_11	5.04	0.038	0.3464	0.0022	1942.0	12.3	1732.1	9.2	-12.1	1732
ES_1_12	3.591	0.038	0.2806	0.0023	1604.0	12.8	1489	16	-7.7	1489
ES_1_13	3.732	0.023	0.2792	0.0015	1589.2	8.3	1568.6	8.2	-1.3	1569
ES_1_14	5.262	0.037	0.3495	0.0021	1950.5	11.7	1799	10	-8.4	1799
ES_1_15	3.209	0.027	0.2641	0.0017	1520.3	9.5	1395	14	-9.0	1395
ES_1_16	3.208	0.026	0.2633	0.0018	1515.1	10.1	1403	11	-8.0	1403
ES_1_17	3.171	0.024	0.2602	0.0014	1497.9	7.9	1404	12	-6.7	1404
ES_1_18	0.1109	0.0039	0.01555	0.00022	99.0	1.4	220	59	7.0	99
ES_1_19	5.658	0.045	0.3563	0.0023	1975.5	12.8	1889	11	-4.6	1889
ES_1_20	3.322	0.055	0.2722	0.0032	1564.7	18.0	1407	27	-11.2	1407
ES_1_21	3.853	0.045	0.2933	0.0024	1669.5	13.4	1541	19	-8.3	1541
ES_1_22	1.022	0.014	0.11661	0.0009	710.4	5.4	739	26	0.5	710
ES_1_23	3.824	0.037	0.2975	0.0023	1696.1	12.9	1504	16	-12.8	1504
ES_1_24	2.322	0.02	0.2175	0.0014	1275.6	8.0	1149	16	-11.0	1149
ES_1_25	2.915	0.035	0.2512	0.0026	1454.3	14.6	1315	14	-10.6	1315
ES_1_26	5.285	0.058	0.3452	0.0027	1922.5	15.0	1834	18	-4.8	1834
ES_1_27	3.187	0.023	0.2645	0.0015	1523.1	8.4	1383	14	-10.1	1383

ES_1_28	3.223	0.031	0.2685	0.0016	1545.7	9.0	1383	16	-11.8	1383
ES_1_29	6.449	0.052	0.3931	0.0028	2167.6	15.8	1962	11	-10.5	1962
ES_1_30	3.17	0.027	0.2604	0.0018	1499.2	10.1	1400	13	-7.1	1400
ES_1_31	1.84	0.023	0.1839	0.0013	1091.3	7.5	1017	26	-7.3	1017
ES_1_32	5.28	0.045	0.3536	0.0022	1974.1	12.3	1791	13	-10.2	1791
ES_1_33	3.713	0.037	0.2732	0.0023	1553.0	12.8	1602	16	3.1	1602
ES_1_34	1.79	0.052	0.18	0.0026	1070.3	15.1	971	58	-10.2	971
ES_1_35	4.026	0.05	0.3102	0.0039	1763.7	21.7	1534	12	-15.0	1534
ES_1_36	3.904	0.054	0.2995	0.0035	1704.8	19.5	1528	14	-11.6	1528
ES_1_37	3.592	0.047	0.2867	0.0028	1640.8	15.7	1453	21	-12.9	1453
ES_1_38	3.366	0.033	0.2732	0.002	1566.9	11.2	1444	15	-8.5	1444
ES_1_39	3.366	0.042	0.266	0.0026	1524.0	14.5	1481	19	-2.9	1481
ES_1_40	2.269	0.02	0.2141	0.0014	1257.0	8.0	1136	17	-10.7	1136
ES_1_41	2.333	0.019	0.2164	0.0013	1268.1	7.4	1173	13	-8.1	1173
ES_1_42	0.3613	0.0083	0.0506	0.00049	318.3	3.1	290	50	-1.9	318
ES_1_43	0.446	0.013	0.0568	0.0012	354.4	7.4	509	31	5.4	354
ES_1_44	5.408	0.057	0.3431	0.0026	1904.6	14.5	1875	19	-1.6	1875
ES_1_45	6.322	0.099	0.3671	0.0043	2010.9	23.7	2047	23	1.8	2047
ES_1_46	3.058	0.044	0.2575	0.0023	1486.7	12.9	1348	20	-10.3	1348
ES_1_47	5.368	0.047	0.3604	0.0024	2012.1	13.4	1790	11	-12.4	1790
ES_1_48	5.362	0.06	0.3506	0.0035	1950.5	19.4	1845	17	-5.7	1845
ES_1_49	5.126	0.057	0.3532	0.0027	1978.1	15.2	1743	17	-13.5	1743
ES_1_50	1.78	0.026	0.1792	0.0015	1065.4	8.7	996	29	-7.0	996
ES_1_51	3.253	0.048	0.2658	0.0027	1526.6	15.2	1429	28	-6.8	1429
ES_1_52	2.816	0.025	0.243	0.0015	1408.7	8.5	1313	15	-7.3	1313
ES_1_53	5.334	0.044	0.3486	0.0024	1941.2	13.3	1830	11	-6.1	1830
ES_1_54	0.0697	0.0016	0.01038	0.0001	66.5	0.6	139	48	2.9	66
ES_1_55	3.793	0.032	0.2872	0.0025	1634.0	13.8	1560.8	9.9	-4.7	1561
ES_1_56	3.473	0.034	0.279	0.0024	1599.5	13.4	1438	12	-11.2	1438
ES_1_57	7.47	0.85	0.367	0.01	1987.5	57.9	1997	82	0.5	1997
ES_1_58	3.718	0.09	0.2847	0.0045	1620.5	25.3	1550	48	-4.5	1550
ES_1_59	3.324	0.03	0.2743	0.002	1577.0	11.2	1393	16	-13.2	1393

ES_1_60	3.353	0.067	0.2759	0.0038	1585.3	21.4	1397	34	-13.5	1397
ES_1_61	3.265	0.048	0.2705	0.0027	1555.3	15.2	1397	28	-11.3	1397
ES_1_62	3.908	0.073	0.3063	0.0046	1745.2	25.7	1499	21	-16.4	1499
ES_1_63	1.894	0.017	0.1879	0.0013	1114.0	7.5	1024	15	-8.8	1024
ES_1_64	4.03	0.034	0.3051	0.0021	1733.5	11.7	1554	11	-11.6	1554
ES_1_65	2.579	0.035	0.2318	0.0021	1352.3	11.9	1216	24	-11.2	1216
ES_1_66	3.986	0.036	0.3042	0.0025	1730.4	13.9	1536	11	-12.7	1536
ES_1_67	0.0826	0.0038	0.0127	0.00021	81.3	1.4	103	93	-1.0	81
ES_1_68	3.323	0.056	0.2708	0.0026	1555.9	14.7	1411	29	-10.3	1411
ES_1_69	0.7494	0.0076	0.09329	0.00067	575.5	4.0	542	22	-1.4	575
ES_1_70	5.391	0.05	0.3535	0.0028	1970.8	15.6	1812	11	-8.8	1812
ES_1_71	3.296	0.07	0.2452	0.0041	1400.3	22.7	1579	27	11.3	1579
ES_1_72	4.49	0.45	0.331	0.025	1883.2	140.5	1501	29	-25.5	1501
ES_1_73	3.305	0.039	0.2701	0.0023	1553.7	12.9	1391	19	-11.7	1391
ES_1_74	3.37	0.036	0.2742	0.002	1575.7	11.2	1403	19	-12.3	1403
ES_1_75	3.5	0.041	0.2799	0.0022	1604.1	12.4	1443	20	-11.2	1443
ES_1_76	3.333	0.047	0.2689	0.0028	1544.3	15.7	1422	22	-8.6	1422
ES_1_77	2.661	0.029	0.2408	0.0026	1403.2	14.6	1208	12	-16.2	1208
ES_1_78	5.2	0.1	0.3316	0.0052	1843.1	28.4	1868	15	1.3	1868
ES_1_79	3.301	0.034	0.2701	0.0022	1553.5	12.3	1394	16	-11.4	1394
ES_1_80	3.038	0.039	0.261	0.0026	1509.8	14.6	1305	16	-15.7	1305
ES_1_81	2.98	0.031	0.2557	0.0024	1480.3	13.5	1303	13	-13.6	1303
ES_1_82	2.713	0.05	0.2361	0.0031	1372.3	17.4	1273	23	-7.8	1273
ES_1_83	5.699	0.051	0.3705	0.0028	2062.6	15.7	1827	11	-12.9	1827
ES_1_84	2.672	0.048	0.2228	0.0035	1290.9	19.7	1378	40	6.3	1378
ES_1_85	3.8	0.056	0.296	0.003	1688.6	16.7	1494	19	-13.0	1494
ES_1_86	3.311	0.049	0.2701	0.0026	1553.2	14.6	1400	23	-10.9	1400
ES_1_87	5.601	0.059	0.365	0.003	2033.1	16.8	1820	14	-11.7	1820
ES_1_88	1.968	0.081	0.1947	0.0041	1152.8	23.7	976	83	-18.1	976
ES_1_89	3.439	0.045	0.2812	0.0028	1615.4	15.7	1396	19	-15.7	1396
ES_1_90	3.364	0.033	0.2762	0.0021	1587.6	11.8	1393	16	-14.0	1393
ES_1_91	3.794	0.044	0.2847	0.003	1620.2	16.6	1558	15	-4.0	1558

ES_1_92	3.831	0.041	0.2951	0.0023	1681.3	12.8	1519	15	-10.7	1519

Table 2. Detrital zircon dating results for Mount All Member sample ES_3. Only grains with discordance magnitude less than 10% are used in final interpretations and probability density plots. Shaded rows indicate > 10% discordance.

Sample	$^{207}Pb/^{235}U$ ratio	2σ abs error	$^{206}Pb/^{238}U$ ratio	2σ abs error	$^{206}Pb/^{238}U$ age	2σ abs error	$^{207}Pb/^{206}Pb$ age	2σ abs error	Percent Discordant	Preferred age
ES_3_1	3.95	0.21	0.2727	0.0029	1542.9	17.3	1610	51	4.2	1610
ES_3_2	2.994	0.024	0.2458	0.0014	1418.9	7.8	1388	12	-2.2	1388
ES_3_3	2.919	0.041	0.2419	0.002	1398.1	11.3	1372	26	-1.9	1372
ES_3_4	5.598	0.042	0.3503	0.0021	1941.6	11.6	1896	11	-2.4	1896
ES_3_5	3.041	0.028	0.2498	0.0017	1440.8	9.5	1397	16	-3.1	1397
ES_3_6	0.0602	0.0034	0.00865	0.00014	55.3	0.9	210	110	7.2	55
ES_3_7	3.079	0.03	0.2497	0.0017	1438.1	9.5	1421	16	-1.2	1421
ES_3_8	2.587	0.059	0.2046	0.0043	1183.5	24.0	1463	18	19.1	1463
ES_3_9	3.019	0.026	0.2476	0.0015	1427.8	8.4	1401	13	-1.9	1401
ES_3_10	2.901	0.034	0.241	0.0016	1393.2	9.0	1379	20	-1.0	1379
ES_3_11	5.013	0.04	0.3338	0.0023	1865.5	12.7	1787	12	-4.4	1787
ES_3_12	3.755	0.029	0.2853	0.0017	1625.0	9.5	1543	13	-5.3	1543
ES_3_13	3.194	0.026	0.2556	0.0014	1468.6	7.8	1449	13	-1.3	1449
ES_3_14	3.557	0.027	0.2696	0.0016	1537.3	8.9	1557	12	1.3	1557
ES_3_15	4.95	0.036	0.3274	0.0019	1828.9	10.5	1802.2	8.7	-1.5	1802
ES_3_16	1.802	0.03	0.1759	0.0016	1043.8	9.3	1055	32	1.1	1055
ES_3_17	5.041	0.049	0.3294	0.0022	1837.0	12.2	1820	16	-0.9	1820
ES_3_18	3.099	0.03	0.253	0.0016	1457.2	9.0	1411	16	-3.3	1411
ES_3_19	5.618	0.041	0.355	0.0024	1969.2	13.3	1882.3	9.7	-4.6	1882
ES_3_20	3.134	0.029	0.2576	0.0018	1484.3	10.1	1391	16	-6.7	1391
ES_3_21	3.063	0.038	0.2522	0.002	1453.7	11.2	1399	21	-3.9	1399
ES_3_22	3.25	0.11	0.2563	0.0049	1471.0	27.4	1466	45	-0.3	1466
ES_3_23	2.901	0.037	0.2428	0.0019	1404.2	10.7	1358	24	-3.4	1358
ES_3_24	2.81	0.11	0.2247	0.0045	1298.2	25.5	1426	67	9.0	1426
ES_3_25	3.09	0.028	0.2544	0.0019	1465.5	10.6	1402	15	-4.5	1402
ES_3_26	3.179	0.036	0.2589	0.002	1490.2	11.2	1410	16	-5.7	1410
ES_3_27	3.27	0.033	0.2638	0.0017	1514.5	9.5	1444	18	-4.9	1444

ES_3_28	3.155	0.021	0.2567	0.0014	1477.6	7.8	1415	11	-4.4	1415
ES_3_29	3.492	0.071	0.2715	0.0029	1553.9	16.4	1483	36	-4.8	1483
ES_3_30	3.258	0.037	0.261	0.0022	1499.4	12.3	1438	22	-4.3	1438
ES_3_31	2.994	0.026	0.2476	0.0016	1429.5	9.0	1378	13	-3.7	1378
ES_3_32	3.188	0.045	0.2553	0.002	1467.4	11.3	1439	22	-2.0	1439
ES_3_33	1.512	0.016	0.15934	0.00093	954.9	5.4	904	21	-2.0	955
ES_3_34	5.226	0.045	0.3421	0.002	1908.5	11.1	1811	13	-5.4	1811
ES_3_35	3.123	0.024	0.2493	0.0014	1434.0	7.8	1443	11	0.6	1443
ES_3_36	3.169	0.028	0.2565	0.0015	1476.9	8.4	1415	14	-4.4	1415
ES_3_37	3.255	0.034	0.2607	0.002	1497.7	11.2	1447	16	-3.5	1447
ES_3_38	3.111	0.024	0.256	0.0016	1476.1	9.0	1380	12	-7.0	1380
ES_3_39	3.083	0.027	0.2505	0.0017	1443.2	9.5	1412	16	-2.2	1412
ES_3_40	3.808	0.097	0.2562	0.0023	1445.8	13.0	1737	38	16.8	1737
ES_3_41	3.795	0.045	0.2844	0.0024	1618.8	13.4	1551	20	-4.4	1551
ES_3_42	5.021	0.041	0.3397	0.0023	1902.5	12.8	1752	12	-8.6	1752
ES_3_43	5.598	0.092	0.348	0.0028	1928.8	15.6	1896	21	-1.7	1896
ES_3_44	3.249	0.043	0.2584	0.0019	1484.8	10.7	1441	22	-3.0	1441
ES_3_45	3.166	0.032	0.2551	0.0019	1467.7	10.6	1428	14	-2.8	1428
ES_3_46	3.735	0.032	0.2846	0.002	1621.6	11.1	1537	13	-5.5	1537
ES_3_47	3.904	0.061	0.2885	0.0029	1639.4	16.2	1571	26	-4.4	1571
ES_3_48	5.237	0.053	0.3453	0.003	1928.2	16.6	1791	12	-7.7	1791
ES_3_49	3.321	0.082	0.2478	0.0021	1418.7	12.0	1503	35	5.6	1503
ES_3_50	4.724	0.046	0.3219	0.0027	1806.9	14.9	1732	12	-4.3	1732
ES_3_51	3.703	0.058	0.2892	0.0032	1652.5	17.9	1478	26	-11.8	1478
ES_3_52	3.78	0.041	0.2838	0.0022	1616.0	12.3	1549	21	-4.3	1549
ES_3_53	3.16	0.026	0.2587	0.0019	1490.8	10.6	1386	12	-7.6	1386
ES_3_54	3.043	0.064	0.2415	0.0059	1390.2	32.8	1454	25	4.4	1454
ES_3_55	3.164	0.049	0.2591	0.0033	1493.7	18.5	1385	28	-7.8	1385
ES_3_56	3.332	0.032	0.2655	0.0019	1524.7	10.6	1438	16	-6.0	1438
ES_3_57	3.415	0.032	0.2727	0.0022	1565.1	12.3	1431	11	-9.4	1431
ES_3_58	5.333	0.05	0.3479	0.0028	1941.3	15.5	1799	12	-7.9	1799
ES_3_59	2.893	0.033	0.2457	0.0019	1423.9	10.7	1308	21	-8.9	1308

ES_3_60	3.366	0.042	0.2694	0.0025	1546.6	14.0	1435	20	-7.8	1435
ES_3_61	5.177	0.037	0.3373	0.0021	1882.7	11.6	1807	11	-4.2	1807
ES_3_62	3.258	0.036	0.2616	0.0019	1504.4	10.7	1424	22	-5.6	1424
ES_3_63	5.206	0.053	0.3476	0.0032	1942.5	17.8	1777	12	-9.3	1777
ES_3_64	3.261	0.041	0.2674	0.0025	1539.2	14.0	1388	20	-10.9	1388
ES_3_65	7.83	0.1	0.4284	0.0044	2334.4	25.2	2129	18	-9.6	2129
ES_3_66	3.289	0.056	0.2672	0.0031	1536.9	17.4	1404	28	-9.5	1404
ES_3_67	4.09	0.12	0.2969	0.0039	1681.8	21.9	1590	39	-5.8	1590
ES_3_68	3.299	0.045	0.2701	0.0028	1552.9	15.7	1406	24	-10.4	1406
ES_3_69	3.256	0.042	0.2613	0.0023	1502.4	12.9	1422	19	-5.7	1422
ES_3_70	5.613	0.054	0.3586	0.0028	1992.5	15.6	1861	15	-7.1	1861
ES_3_71	3.299	0.045	0.267	0.0026	1534.8	14.6	1418	21	-8.2	1418
ES_3_72	5.589	0.051	0.3658	0.003	2040.6	16.8	1800	13	-13.4	1800
ES_3_73	3.316	0.04	0.2686	0.0026	1543.9	14.6	1405	20	-9.9	1405
ES_3_74	3.306	0.042	0.2698	0.0025	1550.6	14.0	1409	19	-10.0	1409
ES_3_75	3.289	0.034	0.2667	0.0023	1533.9	12.9	1406	16	-9.1	1406
ES_3_76	5.393	0.057	0.3532	0.0036	1969.6	20.0	1810	14	-8.8	1810
ES_3_77	3.356	0.04	0.2749	0.0025	1581.5	14.0	1381	19	-14.5	1381
ES_3_78	3.273	0.034	0.2669	0.0024	1535.0	13.4	1400	18	-9.6	1400
ES_3_79	3.271	0.056	0.2726	0.0035	1568.9	19.6	1376	26	-14.0	1376
ES_3_80	7.205	0.078	0.4208	0.0044	2311.9	25.2	2025	13	-14.2	2025
ES_3_81	4.042	0.041	0.3081	0.0028	1751.7	15.6	1538	18	-13.9	1538
ES_3_82	3.544	0.038	0.2858	0.0025	1637.6	14.0	1436	15	-14.0	1436
ES_3_83	3.313	0.047	0.2707	0.0029	1555.9	16.3	1408	25	-10.5	1408
ES_3_84	3.334	0.031	0.2697	0.0016	1549.9	9.0	1412	15	-9.8	1412
ES_3_85	3.877	0.057	0.2987	0.0032	1701.4	17.9	1523	25	-11.7	1523
ES_3_86	5.74	0.11	0.3704	0.004	2058.4	22.6	1839	24	-11.9	1839
ES_3_87	3.375	0.039	0.2773	0.0025	1593.7	14.0	1391	17	-14.6	1391
ES_3_88	3.641	0.079	0.2837	0.0042	1622.7	23.6	1463	38	-10.9	1463
ES_3_89	3.4	0.041	0.277	0.0026	1590.8	14.6	1408	18	**-13.0**	1408

Table 3. Detrital zircon dating results for Murphy's Member sample ES_4. Only grains with discordance magnitude less than 10% are used in final interpretations and probability density plots. Shaded rows indicate > 10% discordance.

Sample	$^{207}Pb/^{235}U$ ratio	2σ abs error	$^{206}Pb/^{238}U$ ratio	2σ abs error	$^{206}Pb/^{238}U$ age	2σ abs error	$^{207}Pb/^{206}Pb$ age	2σ abs error	Percent Discordant	Preferred age
ES_4_1	4.78	0.049	0.3136	0.0028	1751.2	15.4	1820	14	3.8	1820
ES_4_2	6.067	0.043	0.3617	0.0023	1991.5	12.7	1983	10	-0.4	1983
ES_4_3	2.932	0.028	0.2406	0.0016	1389.6	9.0	1390	16	0.0	1390
ES_4_4	3.191	0.034	0.2602	0.0024	1498.3	13.4	1396	14	-7.3	1396
ES_4_5	4.591	0.041	0.3023	0.0027	1691.0	14.7	1806.3	9.1	6.4	1806
ES_4_6	6.044	0.065	0.3631	0.003	2001.1	16.7	1968	17	-1.7	1968
ES_4_7	2.975	0.026	0.2449	0.0014	1413.8	7.9	1387	14	-1.9	1387
ES_4_8	2.866	0.024	0.2385	0.0015	1379.3	8.4	1372	16	-0.5	1372
ES_4_9	3.235	0.064	0.2509	0.0021	1438.9	11.9	1488	32	3.3	1488
ES_4_10	2.44	0.22	0.1157	0.0049	638.0	27.6	2150	130	80.7	638
ES_4_11	2.365	0.032	0.2026	0.0019	1182.2	10.7	1309	21	9.7	1309
ES_4_12	2.712	0.028	0.2283	0.0014	1325.2	7.9	1331	18	0.4	1331
ES_4_13	3.699	0.035	0.2824	0.0022	1610.7	12.3	1524	15	-5.7	1524
ES_4_14	3.333	0.041	0.2685	0.0029	1541.7	16.2	1428	17	-8.0	1428
ES_4_15	3.441	0.04	0.2654	0.002	1518.7	11.2	1505	21	-0.9	1505
ES_4_16	4.812	0.04	0.318	0.0025	1778.8	13.7	1788	11	0.5	1788
ES_4_17	5.171	0.041	0.3411	0.0023	1903.7	12.8	1801	13	-5.7	1801
ES_4_18	5.079	0.043	0.3358	0.0022	1875.8	12.2	1794	11	-4.6	1794
ES_4_19	5.068	0.037	0.3313	0.0023	1849.2	12.7	1807	11	-2.3	1807
ES_4_20	5.752	0.045	0.3556	0.0024	1968.2	13.3	1914	10	-2.8	1914
ES_4_21	4.992	0.046	0.3244	0.002	1810.7	11.1	1809	13	-0.1	1809
ES_4_22	4.735	0.058	0.3094	0.0028	1729.7	15.4	1808	15	4.3	1808
ES_4_23	2.838	0.03	0.2263	0.0021	1306.2	11.7	1445	12	9.6	1445
ES_4_24	4.766	0.039	0.324	0.002	1819.1	11.1	1729	11	-5.2	1729
ES_4_25	3.086	0.042	0.2541	0.0023	1466.9	12.9	1365	21	-7.5	1365
ES_4_26	3.086	0.031	0.2515	0.002	1450.5	11.2	1390	15	-4.4	1390
ES_4_27	5.204	0.059	0.3356	0.0029	1871.1	16.1	1818	19	-2.9	1818

ES_4_28	3.132	0.031	0.2529	0.002	1456.8	11.2	1408	16	-3.5	1408
ES_4_29	3.538	0.051	0.2706	0.0026	1547.7	14.5	1501	25	-3.1	1501
ES_4_30	2.604	0.086	0.2077	0.0074	1202.4	41.3	1447	17	16.9	1447
ES_4_31	3.477	0.062	0.2669	0.0027	1527.9	15.2	1488	30	-2.7	1488
ES_4_32	6.419	0.053	0.3778	0.0024	2077.7	13.4	1997	14	-4.0	1997
ES_4_33	5.332	0.041	0.3381	0.0023	1881.9	12.7	1843.9	9.7	-2.1	1844
ES_4_34	3.166	0.04	0.2542	0.0021	1464.6	11.8	1400	24	-4.6	1400
ES_4_35	3.493	0.054	0.2622	0.0034	1497.5	18.9	1545	24	3.1	1545
ES_4_36	5.45	0.11	0.3438	0.006	1916.3	33.1	1818	20	-5.4	1818
ES_4_37	3.286	0.027	0.2595	0.0017	1491.4	9.5	1434	13	-4.0	1434
ES_4_38	3.121	0.033	0.2491	0.002	1435.0	11.2	1416	19	-1.3	1416
ES_4_39	3.281	0.028	0.2595	0.0018	1492.2	10.1	1424	13	-4.8	1424
ES_4_40	0.894	0.016	0.1058	0.0012	649.4	7.2	618	39	-0.1	649
ES_4_41	5.175	0.036	0.3332	0.002	1858.8	11.0	1815	10	-2.4	1815
ES_4_42	3.267	0.045	0.2565	0.002	1474.2	11.2	1438	20	-2.5	1438
ES_4_43	3.218	0.029	0.2602	0.0017	1499.2	9.5	1385	14	-8.2	1385
ES_4_44	3.563	0.032	0.2766	0.002	1583.0	11.1	1473	12	-7.5	1473
ES_4_45	5.271	0.042	0.3433	0.0025	1916.9	13.9	1795	11	-6.8	1795
ES_4_46	0.7249	0.0091	0.08852	0.00068	546.8	4.1	553	21	1.1	547
ES_4_47	1.844	0.028	0.1812	0.0016	1076.3	9.2	1006	29	-7.0	1006
ES_4_48	3.27	0.047	0.2581	0.0024	1484.8	13.4	1424	21	-4.3	1424
ES_4_49	5.289	0.044	0.3448	0.0024	1925.0	13.3	1796	12	-7.2	1796
ES_4_50	5.263	0.041	0.3362	0.0023	1874.3	12.7	1823	11	-2.8	1823
ES_4_51	5.329	0.056	0.3419	0.0031	1907.2	17.2	1812	14	-5.3	1812
ES_4_52	3.181	0.028	0.2537	0.0021	1461.4	11.7	1407	14	-3.9	1407
ES_4_53	5.152	0.035	0.3336	0.002	1863.7	11.0	1793.3	8.3	-3.9	1793
ES_4_54	3.335	0.045	0.2632	0.0026	1512.8	14.6	1429	22	-5.9	1429
ES_4_55	4.01	0.12	0.2797	0.004	1584.8	22.5	1596	50	0.7	1596
ES_4_56	3.243	0.036	0.2633	0.0023	1516.2	12.9	1387	18	-9.3	1387
ES_4_57	3.253	0.036	0.2616	0.0021	1506.1	11.8	1398	17	-7.7	1398
ES_4_58	3.195	0.032	0.2585	0.002	1490.0	11.2	1380	15	-8.0	1380
ES_4_59	5.016	0.053	0.3345	0.0027	1874.3	15.0	1749	14	-7.2	1749

ES_4_60	3.285	0.048	0.2699	0.003	1555.7	16.8	1352	20	-15.1	1352
ES_4_61	5.433	0.058	0.3551	0.0036	1982.3	20.0	1792	11	-10.6	1792
ES_4_62	5.407	0.069	0.3436	0.0033	1912.7	18.3	1840	19	-3.9	1840
ES_4_63	5.68	0.11	0.3585	0.0034	1993.8	19.1	1833	22	-8.8	1833
ES_4_64	3.246	0.045	0.2635	0.0027	1518.0	15.2	1375	25	-10.4	1375
ES_4_65	4.31	0.089	0.3121	0.0042	1767.4	23.5	1603	34	-10.3	1603
ES_4_66	5.171	0.051	0.3379	0.0025	1888.1	13.9	1788	14	-5.6	1788
ES_4_67	5.608	0.053	0.3621	0.0028	2018.4	15.6	1813	12	-11.3	1813
ES_4_68	3.676	0.035	0.2846	0.0021	1627.0	11.7	1479	16	-10.0	1479
ES_4_69	3.476	0.077	0.256	0.0025	1461.4	14.1	1553	33	5.9	1553
ES_4_70	7.3	0.44	0.2902	0.0054	1502.7	30.9	2544	82	40.9	2544
ES_4_71	3.202	0.034	0.2604	0.0023	1501.3	12.9	1373	15	-9.3	1373
ES_4_72	3.271	0.04	0.266	0.0023	1529.8	12.9	1408	18	-8.6	1408
ES_4_73	3.355	0.039	0.2685	0.0022	1544.0	12.4	1404	21	-10.0	1404
ES_4_74	3.689	0.049	0.2838	0.0026	1620.5	14.5	1496	21	-8.3	1496
ES_4_75	3.505	0.043	0.2749	0.0025	1575.8	14.0	1446	20	-9.0	1446
ES_4_76	3.295	0.038	0.2675	0.0022	1537.8	12.3	1410	17	-9.1	1410
ES_4_77	3.929	0.032	0.2975	0.0021	1694.4	11.7	1525	10	-11.1	1525
ES_4_78	3.467	0.091	0.269	0.0043	1540.2	24.1	1474	43	-4.5	1474
ES_4_79	3.724	0.049	0.2796	0.0035	1593.7	19.5	1525	24	-4.5	1525
ES_4_80	3.602	0.056	0.2786	0.0024	1592.5	13.5	1485	23	-7.2	1485
ES_4_81	3.384	0.049	0.2742	0.0028	1574.6	15.7	1413	22	-11.4	1413
ES_4_82	5.484	0.078	0.3235	0.0039	1783.0	21.1	1990	15	10.4	1990
ES_4_83	5.579	0.059	0.3643	0.0035	2030.3	19.6	1812	16	-12.0	1812
ES_4_84	3.387	0.043	0.274	0.0028	1573.7	15.7	1408	19	-11.8	1408
ES_4_85	6.619	0.074	0.3974	0.0042	2189.9	23.7	1973	15	-11.0	1973
ES_4_86	4.688	0.039	0.31	0.0024	1734.0	13.1	1798.3	9.1	3.6	1798
ES_4_87	6.714	0.089	0.403	0.0046	2221.4	26.0	1970	17	-12.8	1970
ES_4_88	3.348	0.071	0.2661	0.0023	1526.7	13.0	1435	25	-6.4	1435
ES_4_89	4.8	0.38	0.391	0.033	2229.4	193.3	1462	34	-52.5	1462
ES_4_90	2.92	0.057	0.2355	0.0043	1358.1	23.9	1435	17	5.4	1435
ES_4_91	2.779	0.03	0.2392	0.0019	1388.1	10.7	1297	20	-7.0	1297

ES_4_92	3.269	0.032	0.2698	0.0019	1552.3	10.6	1390	14	-11.7	1390
ES_4_93	3.508	0.035	0.2855	0.0023	1636.6	12.9	1427	15	-14.7	1427
ES_4_94	3.56	0.076	0.2858	0.004	1632.9	22.4	1478	36	-10.5	1478

Table 4. Detrital zircon dating results for Walker's Member sample ES_5. Only grains with discordance magnitude less than 10% are used in final interpretations and probability density plots. Shaded rows indicate > 10% discordance.

Sample	$^{207}Pb/^{235}U$ ratio	2σ abs error	$^{206}Pb/^{238}U$ ratio	2σ abs error	$^{206}Pb/^{238}U$ age	2σ abs error	$^{207}Pb/^{206}Pb$ age	2σ abs error	Percent Discordant	Preferred age
ES_5_1	0.827	0.016	0.09881	0.00089	606.4	5.4	649	41	0.8	606
ES_5_2	1.578	0.039	0.1599	0.0025	953.7	14.5	1013	43	0.7	954
ES_5_3	2.827	0.03	0.2374	0.0016	1373.0	9.0	1380	20	0.5	1380
ES_5_4	2.635	0.023	0.2297	0.0016	1335.2	9.0	1298	13	-2.9	1298
ES_5_5	2.917	0.025	0.2461	0.0016	1422.2	9.0	1365	14	-4.2	1365
ES_5_6	0.794	0.041	0.1027	0.002	633.7	12.2	450	100	-6.1	634
ES_5_7	2.686	0.023	0.2332	0.0016	1354.3	9.0	1308	13	-3.5	1308
ES_5_8	7.09	0.51	0.1506	0.0065	627.6	29.8	3533	65	218.0	628
ES_5_9	1.657	0.017	0.1694	0.0011	1009.3	6.4	995	20	-1.4	995
ES_5_10	0.8356	0.0081	0.10233	0.00067	628.4	4.0	615	20	-1.8	628
ES_5_11	0.879	0.013	0.10689	0.00078	655.4	4.7	612	32	-2.3	655
ES_5_12	5.54	0.73	0.0696	0.0097	133.0	72.7	4660	570	1255.4	133
ES_5_13	40.4	4.8	0.409	0.067	506.6	260.1	5030	220	634.3	507
ES_5_14	0.8505	0.0079	0.10411	0.00073	639.0	4.4	616	16	-2.2	639
ES_5_15	1.694	0.021	0.1691	0.0013	1005.5	7.5	1044	25	3.7	1044
ES_5_16	0.8097	0.0094	0.10002	0.00063	614.6	3.8	600	23	-2.1	615
ES_5_17	2.56	0.059	0.1823	0.0029	1045.5	16.1	1682	19	37.8	1682
ES_5_18	0.0934	0.0043	0.01254	0.00014	79.7	0.9	322	77	13.2	80
ES_5_19	0.311	0.011	0.04518	0.00057	285.4	3.6	208	71	-4.4	285
ES_5_20	0.79	0.014	0.0954	0.001	586.3	6.0	632	34	0.8	586
ES_5_21	1.5	0.02	0.1574	0.0013	942.5	7.6	937	24	-1.3	942
ES_5_22	2.361	0.024	0.2176	0.0015	1273.2	8.5	1197	18	-6.4	1197
ES_5_23	1.661	0.013	0.1699	0.0011	1012.2	6.3	997	13	-1.5	997
ES_5_25	4.894	0.047	0.3283	0.0028	1832.8	15.4	1809	11	-1.3	1809
ES_5_26	2.69	0.021	0.2332	0.0014	1353.7	7.9	1314	13	-3.0	1314
ES_5_27	2.746	0.022	0.2374	0.0017	1375.7	9.5	1334	13	-3.1	1334
ES_5_29	4.264	0.068	0.2921	0.0047	1640.5	25.7	1762	14	6.9	1762

ES_5_30	2.593	0.048	0.2249	0.0018	1308.2	10.3	1285	28	-1.8	1285
ES_5_31	0.863	0.019	0.1055	0.001	647.2	6.1	616	51	-2.5	647
ES_5_32	1.658	0.022	0.1697	0.0013	1011.3	7.5	992	26	-1.9	992
ES_5_33	2.46	0.15	0.0359	0.002	89.5	11.9	4260	120	1266.9	89
ES_5_34	5.406	0.041	0.3569	0.0024	1988.5	13.3	1821.9	8.4	-9.1	1822
ES_5_35	3.028	0.05	0.2505	0.003	1443.2	16.8	1408	26	-2.5	1408
ES_5_36	1.729	0.029	0.1748	0.0014	1039.3	8.2	1012	33	-2.7	1012
ES_5_37	0.0849	0.0043	0.0126	0.00021	80.6	1.4	180	97	2.2	81
ES_5_38	3.612	0.042	0.2741	0.0019	1561.6	10.6	1559	18	-0.2	1559
ES_5_39	0.739	0.034	0.01777	0.00049	76.9	2.8	3478	67	623.3	77
ES_5_40	4.976	0.039	0.3377	0.0023	1889.1	12.7	1772.5	9.6	-6.6	1773
ES_5_41	0.2826	0.0034	0.04057	0.00032	256.4	2.0	251	27	-1.4	256
ES_5_42	5.257	0.029	0.3438	0.0017	1915.0	9.4	1831	8.2	-4.6	1831
ES_5_43	0.1812	0.0042	0.02685	0.0003	170.8	1.9	170	46	-1.1	171
ES_5_44	0.899	0.025	0.1058	0.0014	647.5	8.4	674	55	0.2	648
ES_5_45	1.552	0.039	0.02352	0.00051	67.2	3.3	4180	48	1311.4	67
ES_5_47	0.874	0.013	0.1082	0.0011	664.0	6.6	587	25	-4.1	664
ES_5_48	2.878	0.032	0.2508	0.0024	1453.4	13.5	1298	15	-12.0	1298
ES_5_50	1.41	0.14	0.1124	0.0053	665.3	31.3	1220	190	22.7	665
ES_5_51	0.986	0.04	0.113	0.0014	688.7	8.5	681	67	-0.5	689
ES_5_52	3.198	0.031	0.2578	0.002	1481.6	11.2	1442	13	-2.7	1442
ES_5_53	0.261	0.019	0.02946	0.00049	184.0	3.2	550	110	23.9	184
ES_5_54	12.6	2.5	0.146	0.032	105.4	176.7	5100	940	2215.5	105
ES_5_55	3.003	0.043	0.2549	0.0026	1473.6	14.6	1330	25	-10.8	1330
ES_5_56	4.68	0.11	0.2926	0.0043	1626.6	23.6	1899	37	14.3	1899
ES_5_58	0.108	0.0036	0.01522	0.00017	97.0	1.1	257	67	7.4	97
ES_5_59	3.64	0.12	0.0446	0.0015	86.5	9.3	4533	66	1694.4	86
ES_5_60	3.491	0.042	0.2793	0.0027	1600.1	15.1	1447	18	-10.6	1447
ES_5_61	0.8528	0.0082	0.10434	0.00085	640.7	5.1	593	18	-2.2	641
ES_5_62	2.525	0.018	0.2296	0.0015	1340.7	8.5	1202.9	8.1	-11.5	1203
ES_5_63	0.648	0.041	0.05185	0.00075	311.0	4.8	1360	100	59.5	311
ES_5_65	3.858	0.039	0.2955	0.003	1682.1	16.7	1536	12	-9.5	1536

ES_5_66	3.187	0.044	0.2686	0.003	1549.9	16.8	1331	20	-16.4	1331
ES_5_67	0.1561	0.0051	0.02308	0.00026	147.0	1.7	176	63	0.1	147
ES_5_68	1.861	0.035	0.1848	0.002	1096.7	11.6	1012	39	-8.4	1012
ES_5_69	0.0997	0.0036	0.01416	0.0002	90.3	1.3	216	77	6.5	90
ES_5_70	0.892	0.02	0.1056	0.0011	647.1	6.6	626	48	-0.2	647
ES_5_71	2.94	0.034	0.2506	0.0022	1450.5	12.4	1322	21	-9.7	1322
ES_5_72	1.889	0.02	0.192	0.0016	1139.2	9.2	986	16	-15.5	986
ES_5_73	0.959	0.024	0.1056	0.0011	644.2	6.6	783	51	5.7	644
ES_5_74	0.7622	0.009	0.09494	0.00074	585.4	4.5	548	21	-1.9	585
ES_5_75	0.1501	0.0068	0.02244	0.00038	143.0	2.4	145	88	-0.8	143
ES_5_76	2.834	0.042	0.2399	0.0024	1389.6	13.5	1341	27	-3.6	1341
ES_5_77	22.8	5.1	0.365	0.087	1066.3	400.1	4010	470	73.4	4010
ES_5_79	17.59	0.87	0.1601	0.0078	66.5	62.1	5050	120	4269.3	66
ES_5_80	5.119	0.041	0.3454	0.0023	1931.6	12.8	1769	10	-9.2	1769
ES_5_81	5.779	0.049	0.3669	0.0027	2036.6	15.1	1871	12	-8.8	1871
ES_5_82	5.264	0.046	0.3485	0.0027	1946.9	15.0	1785	11	-9.1	1785
ES_5_83	3.29	0.042	0.2662	0.0026	1528.3	14.6	1437	23	-6.4	1437
ES_5_84	1.79	0.18	0.1263	0.0071	731.3	40.9	1500	180	28.4	731
ES_5_85	0.1943	0.0035	0.02828	0.00024	179.7	1.5	188	37	0.4	180
ES_5_86	0.818	0.03	0.0977	0.0015	600.3	9.1	607	78	1.0	600
ES_5_87	3.861	0.036	0.289	0.0021	1642.7	11.7	1570	14	-4.6	1570
ES_5_88	2.676	0.022	0.2291	0.0013	1330.5	7.3	1316	15	-1.1	1316
ES_5_89	3.147	0.022	0.256	0.0015	1474.0	8.4	1411.4	9.3	-4.4	1411
ES_5_90	7	1.3	0.16	0.012	714.7	63.9	3300	180	179.8	715
ES_5_92	0.0881	0.0054	0.01102	0.00033	69.8	2.1	443	67	21.9	70
ES_5_93	3.23	0.14	0.2293	0.0058	1307.3	32.0	1646	37	20.6	1646
ES_5_94	39.8	1.8	0.356	0.021	474.2	65.5	4957	58	693.8	474
ES_5_95	3.8	1.2	0.227	0.076	1235.2	422.3	1900	1000	35.0	1900
ES_5_96	0.481	0.061	0.01364	0.00064	66.5	4.0	2800	170	426.6	66